Article

Design and Experimentation of the Millet Combine Harvester Header

Shujin Qiu [1,2], Kai Li [1,2], Yifan Hu [3], Ben Pan [1,2], Zeze Wang [1,2], Xiangyang Yuan [4], Qingliang Cui [1,2,*] and Zhong Tang [3]

1 College of Engineering, Shanxi Agricultural University, Taigu 030801, China; qiushujin@sxau.edu.cn (S.Q.); s20212068@stu.sxau.edu.cn (K.L.); s20222072@stu.sxau.edu.cn (B.P.); z20223005@stu.sxau.edu.cn (Z.W.)
2 Dryland Farm Machinery Key Technology and Equipment Key Laboratory of Shanxi Province, Taigu 030801, China
3 School of Agricultural Engineering, Jiangsu University, Zhenjiang 212013, China; 2222216038@stmail.ujs.edu.cn (Y.H.); zht@ujs.edu.cn (Z.T.)
4 College of Agriculture, Shanxi Agricultural University, Taigu 030801, China; yuanxiangyang200@sxau.edu.cn
* Correspondence: cuiqingliang@sxau.edu.cn

Abstract: To address the issue of header loss in millet combine harvesters, a double-chain millet harvester header was designed based on the principles of contact mechanics and tribology. Key component parameters of the header were determined, with the divider length and width measuring 0.56 m and 0.30 m, respectively. The divider angle was 40°, and the spiral angle was also 40°. A prototype was manufactured, and field performance tests were conducted. The results showed that the total header loss rate of the double-chain header was lower than that of the single-chain header under various combinations of header height and harvesting speed. The lowest total header loss rate, 3.12%, occurred when the header height was 0.2 m and the harvesting speed was 1.667 m/s, with a grain loss rate of 0.55% and a spike loss rate of 2.57%. This research provides a theoretical foundation for the development of low-loss, high-efficiency millet combine harvesters.

Keywords: millet harvester; divider; header height; harvesting speed; header loss rate

1. Introduction

The planting area of foxtail millet in China is 839.76 thousand hectares, accounting for over 80% of the global area. Millet is an important export and foreign exchange earning product for China, and its market demand has gradually increased in recent years [1,2]. The application of grain combine harvesters is becoming increasingly widespread, which is of great significance for maintaining national food security [3–6]. At present, there is no special harvester for millet due to the special biomechanical characteristics of foxtail millet, such as a high stem height and easy shedding of grains, and millet harvesting operations have the problem of a high loss rate [7,8]. The total loss rate of millet using combined harvesting is 9.40%, more than twice that of manual harvesting (3.51%) [9]. Header loss is the most significant part of the total loss in millet harvesting operations. The outdated millet harvesting equipment hinders the development of the millet industry, making it urgent to develop a low-loss, high-efficiency millet harvester header [10–12].

There are two main types of grain harvester headers according to the lifting mechanism, vertical and horizontal headers, and current research has mostly focused on reel-type headers. For example, the 4LZG-3.0 millet combine harvester (Xingguang Agricultural Machinery Co., Ltd, Huzhou, China) was designed featuring a millet-specific reel-type header, which effectively reduced the side hanging and shedding of panicles during harvesting by improving the dividers on both sides of the header [13]. The vibration analysis and structural optimization on the reel-type millet combine harvester header frame effectively prevented resonance during operation of the combine harvester, thereby

reducing the header loss rate [14]. Wang et al. investigated the positional parameters of the triangular area between the reel, auger, and cutter bar and their impact on the performance of the header. They optimized the parameters of this triangular area between the reel, auger, and cutter bar. The improved header effectively reduced the phenomenon of material accumulation [15]. Li designed the overall structure and major components of low-loss headers for millet combine harvesters. Through simulation software, they simulated the threshing process of millet stalks with header dividers and optimized divider parameters. Field validation tests showed that both header paddle loss rates and divider loss rates met performance criteria [16]. Zhang designed the dividing mechanism of the header for the millet combine harvester, developed and conducted motion simulations for the reel, and performed static and modal analyses of the header frame. However, field trial validations were not completed [17]. The reel-type header is advantageous in lifting lodged crops and reducing impacts on the heads of the crops. However, due to the constant downward orientation of the reel fingers during their movement, it tends to have issues, such as entanglement and crop hanging, especially with taller plants [18]. Scholars have also conducted extensive research on the harvester headers of crops such as soybeans, rapeseed, peanuts, safflower, corn, and sunflowers, achieving phased results [19–24].

Liu et al. designed an adaptive profiling header that can accurately perceive terrain changes and adaptively adjust the height and horizontal angle of the header [25]. Pang et al. measured and analyzed the time-domain and frequency-domain characteristics of the vibration response of the three connection points between the cutting blade system and the cutting platform of a combine harvester. They found that the blade groove was the main vibration source and designed a nut with a rubber sleeve to reduce the vibration transmitted from the blade to the blade groove [26]. Ma et al. conducted field experiments during the rice harvest period to study the effects of factors such as harvest time and temperature on the static friction coefficient of rice stems and grains [27]. In countries with small planting areas, millet is generally used as pasture, and there is relatively little research on mechanical harvesting of millet grains [16].

Currently, the research on millet combine harvester headers primarily focuses on anti-clogging structure design, optimization of motion parameters, and vibration analysis. However, studies addressing the reduction in harvesting losses in chain-tooth millet combine harvester headers have not yet been reported. This study presents the design of a double chain-tooth millet combine harvester header that efficiently feeds millet stems through a double chain-tooth threshing mechanism. The design optimizes the spatial distribution and motion parameters of the stems and ears within the header, reducing ear loss, stem entanglement, and blockages. This provides a foundation for the development of low-loss, efficient millet combine harvesters.

2. Materials and Methods

2.1. Millet Mechanical Properties

The Zhangza 13 millet was selected as the research object, which has a high yield and wide planting area. A mulching hole sowing planting mode with a row spacing of 0.5 m and a hole spacing of 0.08 m was adopted in Fanshi, Shanxi. The biological and mechanical properties of the mature millet were tested; the stem moisture content was 59.4%~76.9%, and the results are shown in Table 1.

2.2. Design of Key Header Components

2.2.1. Design of Divider Length

As the harvester moves forward, the divider shifts from position 1 to position 2. The chain finger moves backward relative to the divider, thereby lifting the lodged millet plants. The process of lifting the lodging millet plant by the chain finger is shown in Figure 1.

Table 1. Biological and mechanical properties of millet.

Parameters	Mean Value	Range
Plant length, m	1.50	1.23~1.68
Stem length, m	1.20	0.94~1.36
Intersection height, m	1.03	0.82~1.25
Approximate grain density, kg·m^{-3}	42.31	31.92~55.18
Critical bending angle of millet stems, °	40.51	29.3~62.5
Friction angle between millet plants and common materials, °	30.88	19.7~52.2
Central bending limit load of stems, N	63.36	56.84~72.47
Lower bending limit load of stems, N	134.08	126.38~144.54

$$\text{The divider length} \quad \begin{cases} S = S_1 + S_2 + a \\ S_1 = vt \\ S_2 = (v_0 - v)t \end{cases} \tag{1}$$

where S = divider length, m; S_1 = displacement of the divider relative to the ground, m; S_2 = displacement of the finger relative to the ground, m; a = finger width, set as 0.03 m; v_0 = chain finger absolute velocity, m·s^{-1}; v = velocity of the harvester, m·s^{-1}; t = time, s; and h = header height, m.
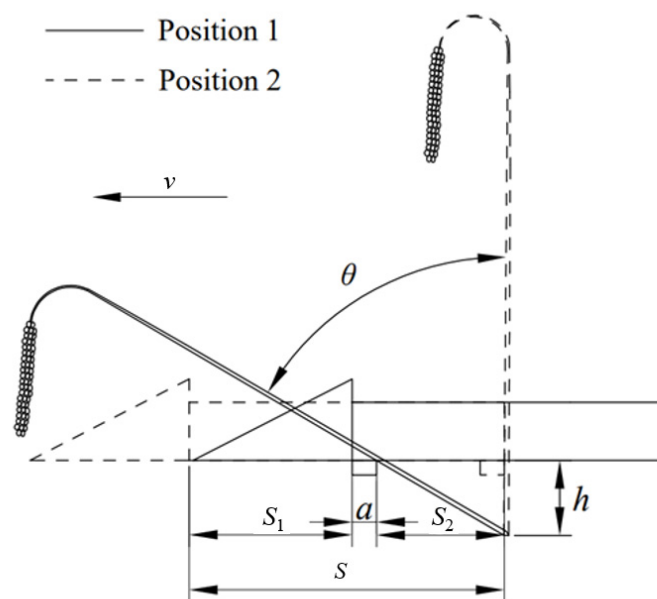
Figure 1. Schematic diagram of the process of the chain finger lifting the lodged millet plant.

Regarding the harvesting of lodging millet, the lower the header height, the easier to lift the lodging millet plants, and the header height h was set as 0.2 m. According to Table 1, the lodging angle θ of the millet plant was taken as 60°, the velocity of the harvester was selected as 3.8 m·s^{-1}, and the absolute velocity v_0 of the chain finger was 4 m·s^{-1}. According to Equation (1), the S was 0.558 m and rounded to 0.56 m.

2.2.2. Design of Divider Width

The row independent feed-in method is generally adopted in millet harvesting. Point A in Figure 2a represents the relative position of the millet plants at the maximum dividing position when the harvester moves forward, moving from point A to point B, and the tilting state of the millet plants is shown in Figure 2b.
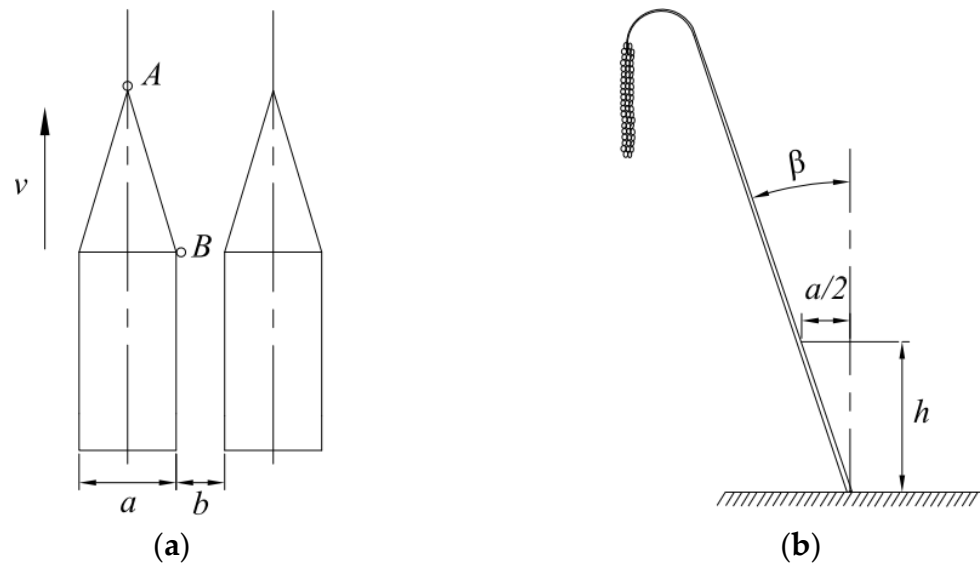
Figure 2. Schematic diagram of the position relationship between the divider and the millet plant. (**a**) Schematic diagram of adjacent dividers; (**b**) Schematic diagram showing the maximum tilting angle of the millet plant.

In order to ensure that the millet plant will not break before entering the gap of the divider, the maximum inclination angle β should be less than the critical breaking angle of the millet plant α:

$$\beta = \arctan\frac{a}{2h} \leq \alpha \tag{2}$$

where β = the maximum tilting angle of the millet plant, (°); α = the critical breaking angle of the millet plant, taken as 30° based on Table 1; a = the divider width, m; and h = the header height, m.

During normal harvesting, the header height should be approximately 0.3 m, and the width of the divider should be less than 0.346 m according to the Equation (2), rounded to 0.30 m.

2.2.3. Design of Divider Angle

As the harvester moves forward, the millet plant moves along the divider. The force diagram of the millet plant separation process is shown in Figure 3, where *o-o'* represents the millet plant.

During the separation process, the relationship between the divider and the millet stalks can be expressed as Equation (3):

$$\begin{cases} F_X + f_{XY}\cos\gamma = ma_X \\ F_Y + f'_{YZ} - f'_{XY} = ma_Y \\ F_Z + mg - f_{YZ}\sin\omega = ma_Z \\ F_X = F_Y\tan\gamma \\ F_Z = F_Y\frac{1}{\tan\omega} \\ f'_{XY} = f_{XY}\sin\gamma = \tan\varphi\sin\gamma\sqrt{F_X^2 + F_Y^2} \\ f'_{YZ} = f_{YZ}\cos\omega = \tan\varphi\sin\omega\sqrt{F_Y^2 + F_Z^2} \\ F = \sqrt{F_X^2 + F_Y^2 + F_Z^2} \end{cases} \tag{3}$$

where F_X = component of the thrust force acting on the particle in the X-direction, N; F_Y = component of the thrust force acting on the particle in the Y-direction, N; F_Z = component of the thrust force acting on the particle in the Z-direction, N; f_{XY} = component of the frictional force acting on the particle in the XOY plane, N; f_{YZ} = component of the frictional

force acting on the particle in the *YOZ* plane, N; f'_{XY} = component of the frictional force f_{XY} in the *Y*-direction, N; f'_{YZ} = component of the frictional force f_{YZ} in the *Y*-direction, N; ω = angle between the tangential line at the contact point and the ground, (°); 2γ = angle of division, (°); φ = angle of friction between the millet stalk and the rigid material, (°); a_X = particle's acceleration component in the *X*-direction, m·s^{-2}; a_Y = particle's acceleration component in the *Y*-direction, m·s^{-2}; and a_Z = particle's acceleration component in the *Z*-direction, m·s^{-2}. Solving Equation (3) yields Equation (4):

$$\begin{cases} a_X = \dfrac{F(\tan\gamma + \tan\varphi)}{m\sqrt{1+\cot^2\omega+\tan^2\gamma}} \\ a_Y = \dfrac{F[1+\tan\varphi(\tan\gamma+\cot\omega)]}{m\sqrt{1+\cot^2\omega+\tan^2\gamma}} \\ a_Z = \dfrac{F(\cot\varphi-\tan\omega)}{m\sqrt{1+\cot^2\varphi+\tan^2\gamma}} + g \end{cases} \tag{4}$$

As per Equation (4), the divider angle 2γ, the friction angle (φ) between the millet stalks and steel material, and the angle (ω) between the tangent at the contact point and the ground are the primary factors influencing the dividing effect. During the harvesting process of millet, the small angle of grain separation leads to an increase in the longitudinal length of the harvester, which affects its flexibility [28]. The excessive angle of grain separation causes the cutting platform to push down the millet plants during harvesting [29]. Taking these factors into account, the divider angle 2γ was chosen to be 40°.
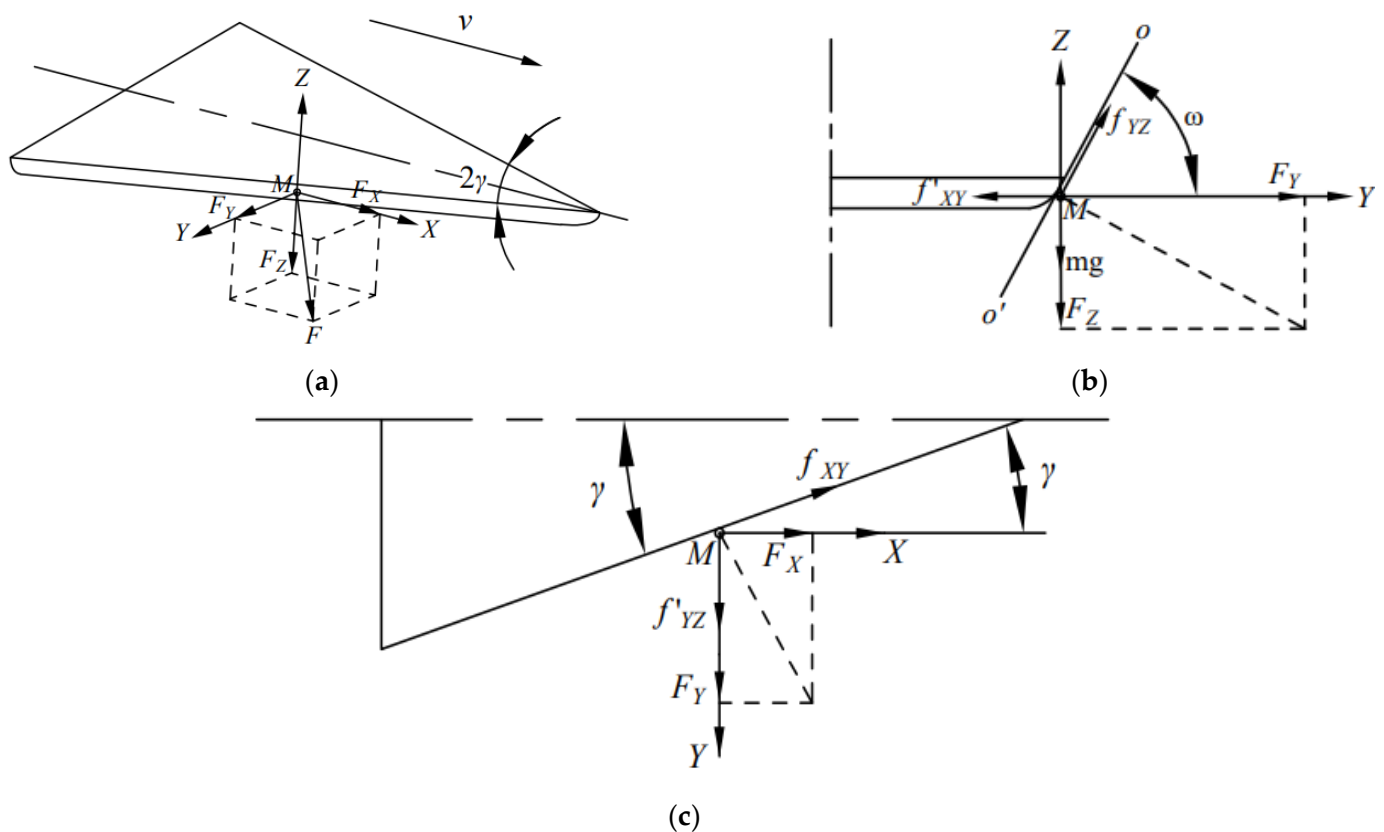

Figure 3. The force analysis schematic of the millet plant separation process. (**a**) Simplified diagram of millet stalks under force; (**b**) Left view; (**c**) Top view.

2.2.4. Parameter Design of the Grain-Lifting Cone

The rationality of the design angle of the grain-lifting cone directly affects its grain separating and lifting capabilities. The grain-lifting cone must not only separate the interwoven millet plants in the field but also possess effective lifting abilities. A larger angle of the grain-lifting cone increases the likelihood of tearing the grain ears, while a smaller angle facilitates the lifting of lodged millet plants but results in a longer header, leading to higher costs.

The shape and installation position of the grain-lifting cone are as depicted in Figure 4. According to Table 1, the interlacing height of the millet plants is between 1.1 and 1.4 m. In line with the findings from related research [16], the angle (ε) between the grain-lifting cone and the ground is designed to be 25°. Consequently, the height H_1 is determined to be 1.6 m.
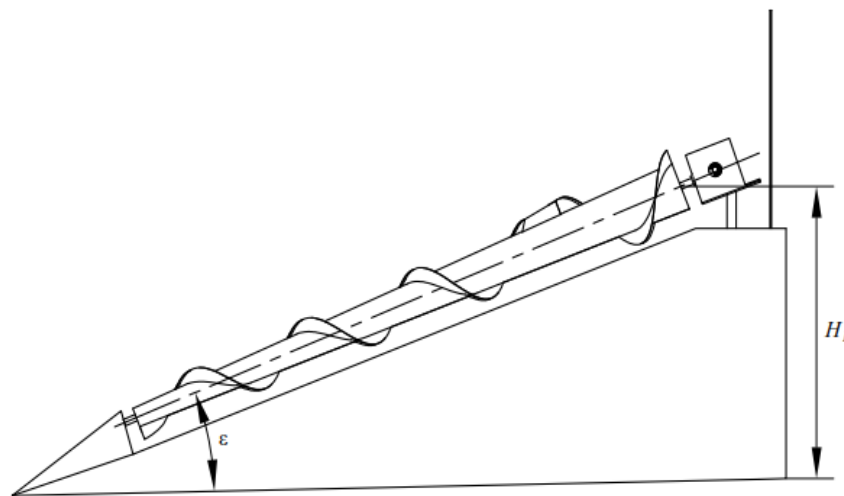

Figure 4. Schematic diagram of grain-lifting cone.

To study the motion state during the contact process between lodged millet stalks and the grain-lifting cone, the stalk unit at point M on the spiral blade of the grain-lifting cone, located at a distance a_1 from the axis, is considered a particle for mechanical analysis [30]. When the helical line is unfolded into a straight-line pp′, the frictional force acts along this line. The force acting on the mass point M of the millet stalks is illustrated in Figure 5.

The interaction between the grain-lifting cone and the millet stalks can be represented by Equation (5):

$$\begin{cases} F'_X - F_f \sin \zeta = ma_X \\ \zeta = \arctan \frac{S_p}{2\pi a_1} \\ F'_X = F_n \cos \zeta \\ F_f = F_n \tan \varphi \end{cases} \tag{5}$$

where F' = total force acting on the mass point, N;

F'_X = axial force acting on the mass point, N;

F_f = frictional force acting on the mass point, N;

ζ = spiral angle, (°);

S_p = spiral blade pitch, m;

a_1 = distance of the mass point from the axis, m.

As can be observed in Figure 5, for the millet stalks to move along the axis, the axial component of the force must exceed the axial frictional force. This is represented in Equation (6):

$$ma_X > 0 \tag{6}$$

The organized result is as follows:

$$\zeta < \frac{\pi}{2} - \varphi \tag{7}$$

According to Equation (7), in order to ensure the millet stalks can be moved axially along the lifting cone, the spiral angle was calculated, and a value of $\zeta = 40°$ was chosen.

Based on the biological and mechanical properties of millet, key components, such as the divider and the grain-lifting cone, were designed.
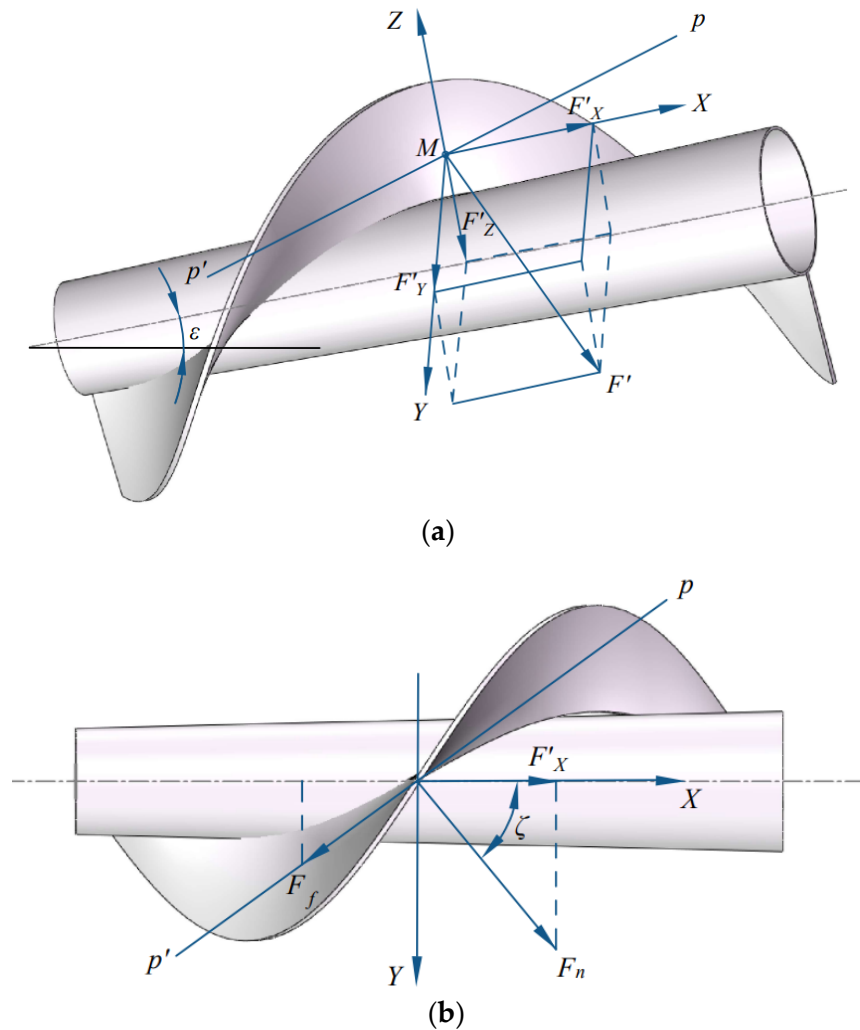

(a)

(b)

Figure 5. The force analysis diagram of millet stalks within the grain-lifting cone. (**a**) Schematic of the force on the millet stalk; (**b**) Z-axis top view.

2.3. Overall Structure and Working Principle of the Header

The header of the double-chain millet harvester was established in the SolidWorks software, which mainly consists of the header frame, grain-lifting cone, screw pusher, baffle, divider, cutting blade, etc., as shown in Figure 6. When the harvester is in operation, the header divides and supports the stalks. The millet plants are passed through the gaps between the dividers and moved to the cutting blade for threshing and cleaning operations. Compared with the traditional harvester header, this structure reduces the entanglement and blockage rate of millet.
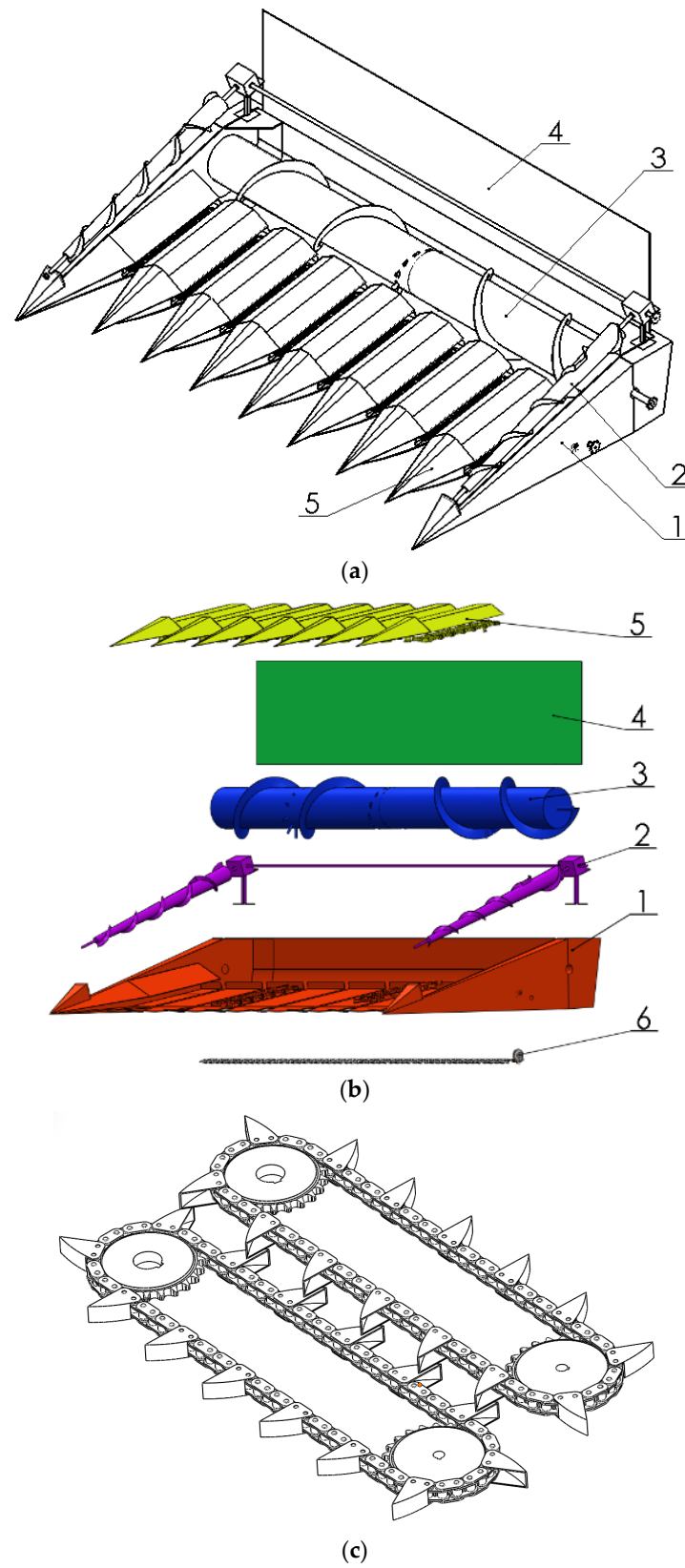
(**a**)

(**b**)

(**c**)

Figure 6. The schematic diagram of the double-chain combine harvester header structure. 1: Header frame; 2: Grain-lifting cones; 3: Spiral conveyor; 4: Baffle plate; 5: Dividers; 6: Cutter. (**a**) Double-chain millet combine harvester header diagram; (**b**) The exploded view of the double-chain millet combine harvester header; (**c**) Schematic diagram of the double-chain structure in a single divider.

2.4. Simulation Model Establishment

During the modeling process, millet stalks were modeled as ellipsoidal flexible bodies with uniform cross-sections. In ADAMS (ADAMS (2024) Hexagon AB, Stockholm, Sweden) [31], a stretching method was used to create the flexible body model of millet stalks. The millet spikes were simplified as cylinders made of a single material, and fixed pairs were added to fix the relative positions of the millet stalks with the millet spikes and the millet stalks with the ground. Customized material parameters for millet plants were defined based on the millet's harvesting mechanical characteristics parameters and data from relevant literature [32,33], as shown in Table 2.

Table 2. Millet plant model parameters.

Parameters	Parameter Values
Length of millet stalks, m	1.23
Length of millet stalk major axis, m	0.0084
Length of millet stalk minor axis, m	0.0066
Density of millet stalks, $(kg \cdot m^{-3})$	480
Young's modulus of millet stalks, MPa	8000
Poisson's ratio of millet stalks	0.33
Length of millet spikes, m	0.271
Radius of millet spikes, m	0.0175
Density of millet spikes, $(kg \cdot m^{-3})$	42.3

The divider head was simplified as a triangular cone structure with a base length of 0.304 m and a width of 0.445 m, and the material of the divider head was defined as steel. The height of the grain divider above the ground was set as an influencing factor at three levels: 0.3 m, 0.4 m, and 0.5 m. The harvesting speed, set as an influencing factor, was designated at three levels: 1.667 m·s^{-1}, 1.111 m·s^{-1}, and 0.556 m·s^{-1}. The simulation was conducted by introducing a moving driver between the divider and the ground.

In the ADAMS software, the impact function method was used to define the collision force between the divider and the millet plants [34]. The impact function method calculates the collision force between two components based on the impact function, which consists of two parts: one is the elastic force generated due to the mutual intrusion of the two components, and the other is the damping force generated due to the relative velocity.

The general expression of the impact function is shown in Equation (8):

$$F_{-impact} = \begin{cases} 0 & q > q_0 \\ k(q_0 - q) - C_{\max}(dq/dt)step(q, q_0, -d, 1, q_0, 0) & q < q_0 \end{cases} \tag{8}$$

where $F_{-impact}$ = collision force between two objects, N;

q_0 = initial distance between the two colliding objects, m;

q = actual distance between the two objects during the collision process, m;

dq/dt = rate of change in distance between the two objects over time, m·s^{-1};

k = stiffness coefficient;

e = collision index;

C_{max} = maximum damping coefficient;

d = penetration depth.

To avoid discontinuities in the damping force during the collision process, a step function was used in the equation, denoted as step (x, x_0, h_0, x_1, h_1) and calculated according to Equation (9):

$$\begin{cases} \Delta = (x - x_0)/(x_1 - x_0) & x \leq x_0 \\ step = \begin{cases} h_0 \\ h_0 + a\Delta^2(3 - 2\Delta) & x_0 < x < x_1 \\ h_1 \end{cases} \\ a = h_1 - h_0 & x \geq x_1 \end{cases} \tag{9}$$

where x = time independent variable, in seconds, s;

x_0 = initial value of the independent variable x;

x_1 = final value of the independent variable x;

h_0 = initial value of the function;

h_1 = final value of the function.

The stiffness coefficient k is typically calculated using the Hertzian elastic collision model theory Formula (10):

$$\begin{cases} k = \sqrt{\frac{16RE^2}{9}} \\ \frac{1}{R} = \frac{1}{R_1} + \frac{1}{R_2} \\ \frac{1}{E} = \frac{(1-\mu_1^2)}{E_1} + \frac{(1-\mu_2^2)}{E_2} \end{cases} \tag{10}$$

where R_1, R_2 = radius of curvature of the two objects at the collision point, m;

E_1, E_2 = elastic modulus of the materials of the two objects, MPa;

μ_1, μ_2 = Poisson's ratio of the materials of the two objects.

The collision parameters were configured as shown in Table 3 [35].

Table 3. Collision parameter settings.

Parameter	Parameter Values
stiffness, (N·m^{-1})	2.10×10^7
damping, (N·s·m^{-1})	0.1
collision index	5
penetration depth, m	0.0001

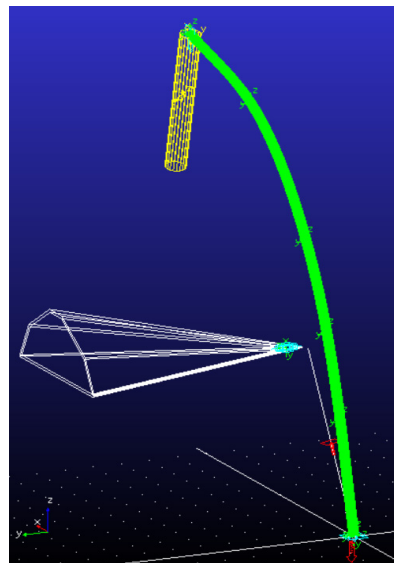The contact model between the divider and millet plants is illustrated in Figure 7.

Figure 7. Millet plant–divider contact model.

2.5. Simulated Experiments

In the simulation experiment involving the contact between the divider and millet plant, the main focus was on studying the structural parameters and operating parameters that affect collision losses. A two-factor, three-level complete experiment [36] was conducted, with the factors being header height (Factor A) denoted as "*h*" and harvesting speed (Factor B) denoted as "*v*". According to the "Quality of Combine Harvesters for Grain (Wheat) Operations" standard (NY/T 995-2006), the lodging degree of millet was categorized as follows: no lodging, moderate lodging, and severe lodging, represented by lodging angles of 0°, 40°, and 70°, respectively. The maximum contact force between the divider and non-lodged plant and the maximum Z-axis contact force between the divider and millet with different lodging degrees were used as indicators to study the influence trends of each factor on the indicators. The simulation experiment aimed to optimize the best design parameters through these simulations.

In the methodology section, the millet biomechanical properties were studied, and key components, such as the divider, grain-lifting cone, and overall structure, were designed. Millet harvester header models were established in SolidWorks, the stress process of key components was analyzed in ADAMS, and optimal parameters were obtained. Finally, the parameters were verified through field experiments.

3. Results

3.1. Experimental Design and Test Results

The factors and their levels for the full-scale experiment are designed as shown in Table 4, and the experimental plan and results are presented in Table 5 and analyzed in Design-Expert (Design-Expert (2024) Stat-Ease, Inc., Minneapolis, MN, USA) [37].

Table 4. Simulation test factors and levels.

Factor Level	Factor A Header Height, m	Factor B Harvesting Speed, $(m \cdot s^{-1})$
1	0.2	0.556
2	0.3	1.111
3	0.4	1.667

Table 5. Simulation test plan and experimental data.

| Number	Experimental Factors		Experimental Indicators		
	Factor A Header Height, m	Factor B Harvesting Speed, $(m \cdot s^{-1})$	The Maximum Contact Force between the Divider and Non-Lodged Millet Plant, N	The Maximum Z-Axis Contact Force for Moderately Lodged Millet Plant, N	The Maximum Z-Axis Contact Force for Severely Lodged Millet Plant, N
1	0.2	0.556	8.63	6.22	3.88
2	0.2	1.111	11.89	11.48	4.46
3	0.2	1.667	12.15	16.46	5.94
4	0.3	0.556	5.01	5.59	0
5	0.3	1.111	6.29	9.28	0
6	0.3	1.667	6.92	16.09	0
7	0.4	0.556	2.78	6.62	0
8	0.4	1.111	4.23	10.63	0
9	0.4	1.667	5.01	15.62	0

The simulation results are shown in (a), (b), and (c) of Figures 8–10; the contact force curves between the divider and millet plant at a header height of 0.2 m, 0.3 m, and 0.4 m are shown, respectively; and the red solid line, the blue dashed line, and the pink dashed line represent the contact force curves between the divider and millet plant at harvesting speeds of 0.556 m·s^{-1}, 1.111 m·s^{-1}, and 1.667 m·s^{-1}, respectively.
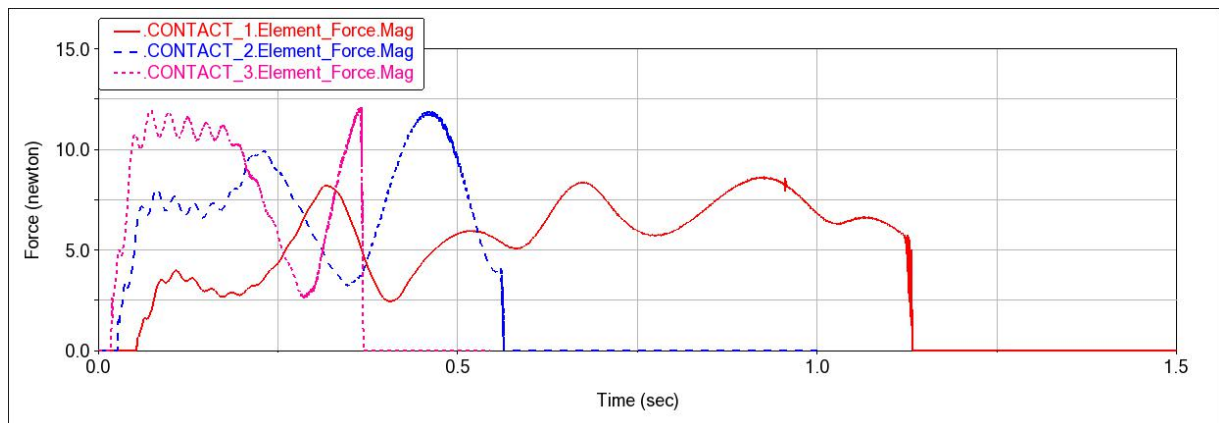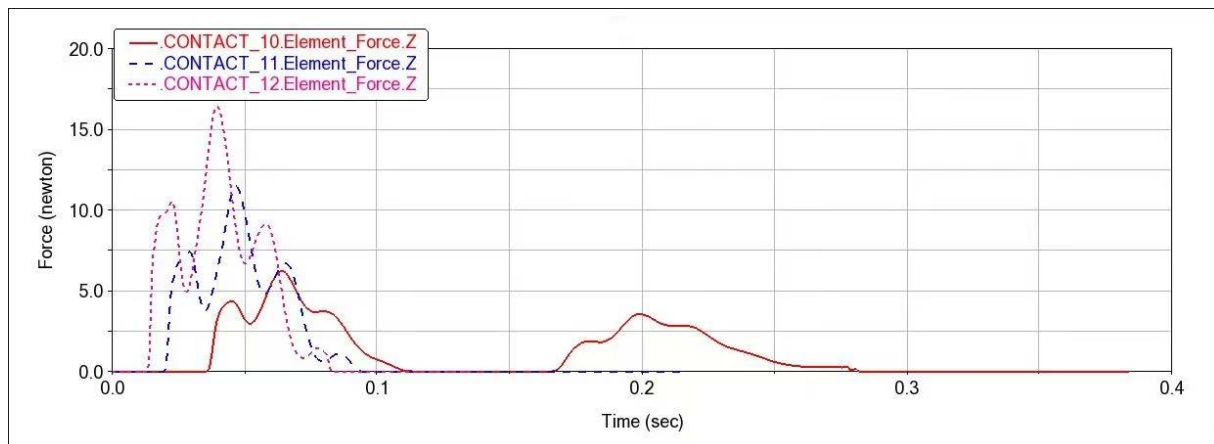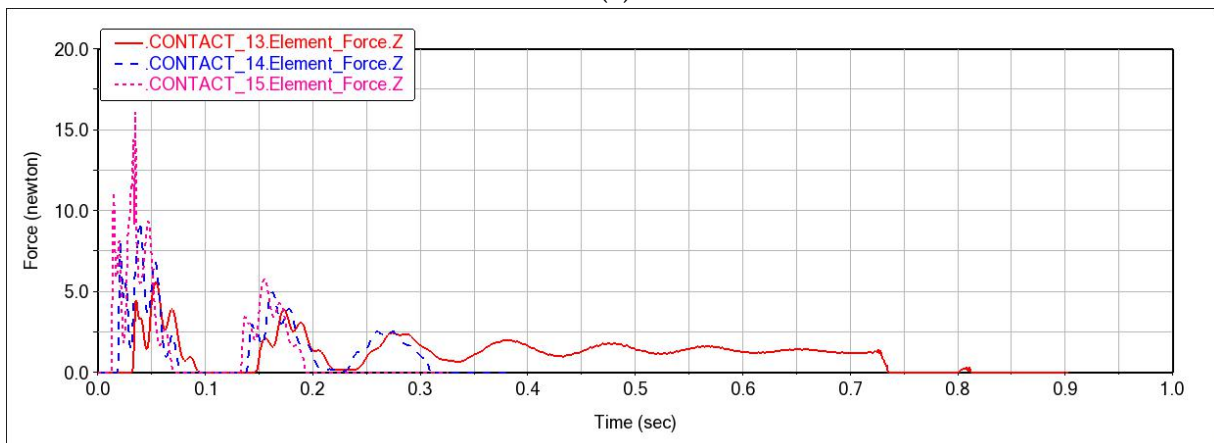
(a)
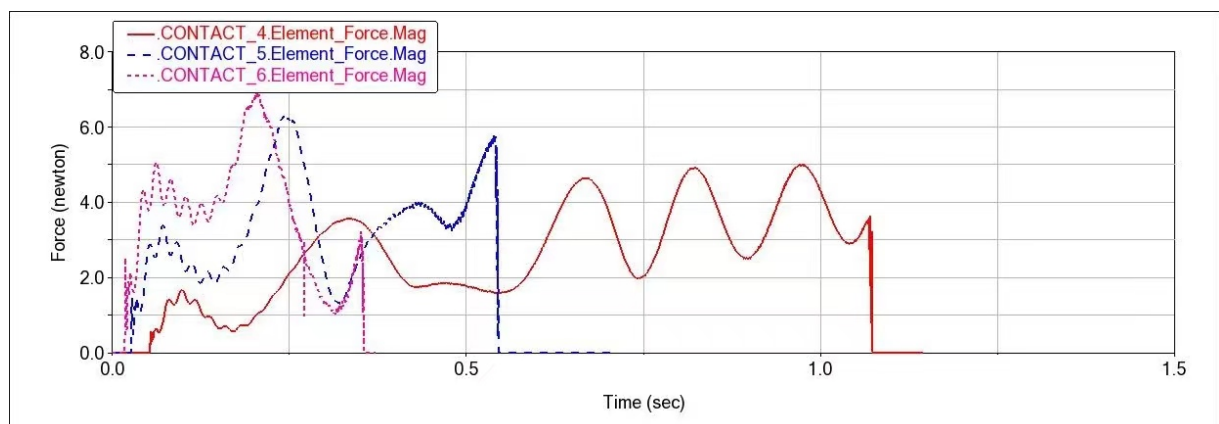
(b)
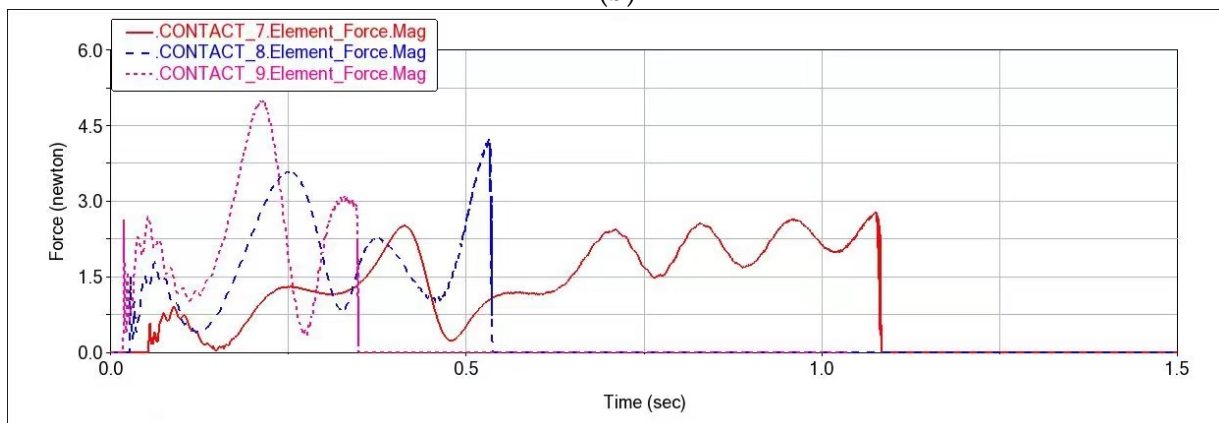
(c)

Figure 8. Simulation diagram of contact force between the divider and non-lodged millet plant. (**a**) At 0.2 m of header height; (**b**) At 0.3 m of header height; (**c**) At 0.4 m of header height.

According to Table 5 and Figure 8, the contact force between the divider and non-lodged millet plant decreases with an increase in the header height. As the harvesting speed increases, the contact force increases. Comparing these results with Table 1, it is evident that, in all simulated test scenarios, the contact forces remained below the bending ultimate load of the millet plant. According to Table 5 and Figure 9, for the Z-axis contact force between the divider and moderately lodged millet plant, there is not a clear pattern of change with increasing header height and increases with higher forward unit speed. According to Table 5 and Figure 10, regarding the Z-axis contact force between the divider and severely lodged millet plant, it increases with higher forward unit speed. Interestingly,
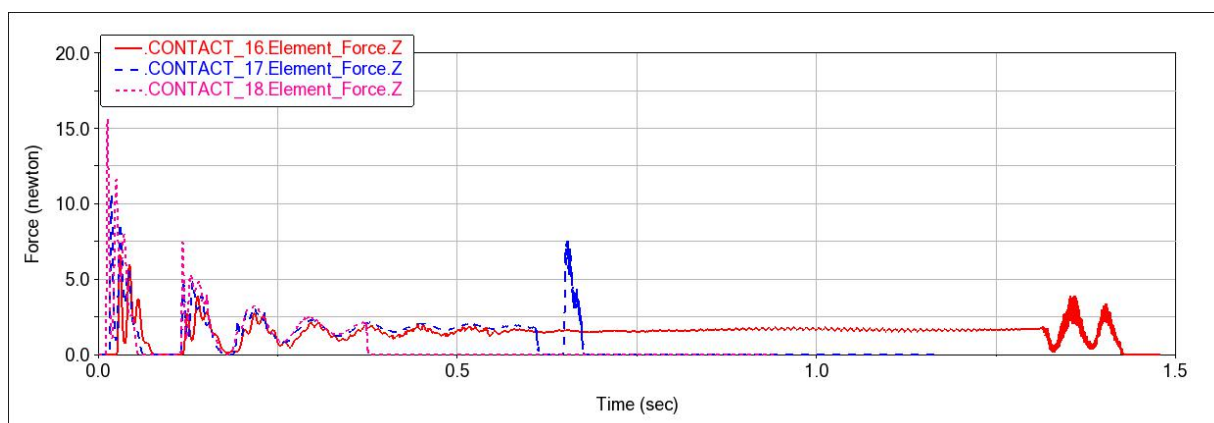
when the header height reaches 0.3 m or 0.4 m, the millet experiences zero *Z*-axis force. This implies that, at a header height of 0.3 m or 0.4 m, the divider is unable to lift severely lodged millet plant.
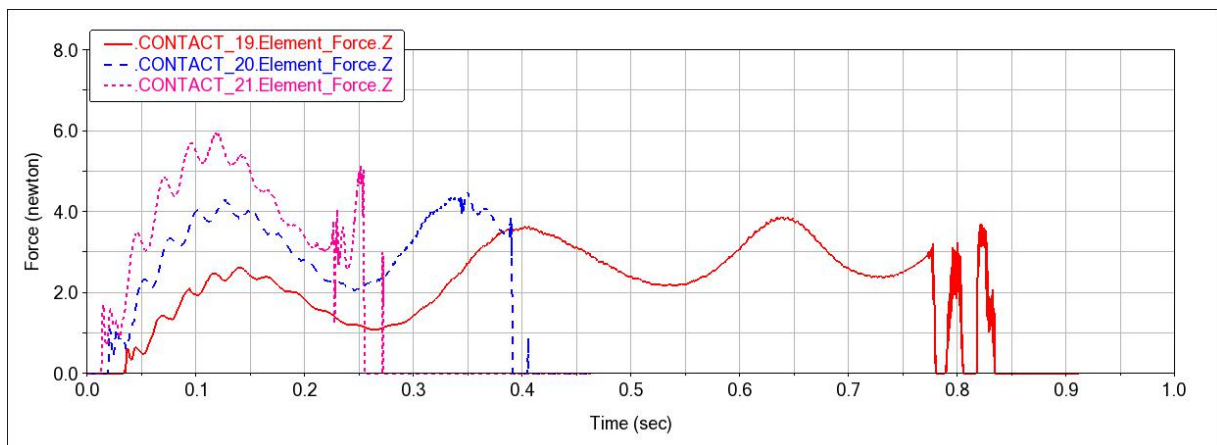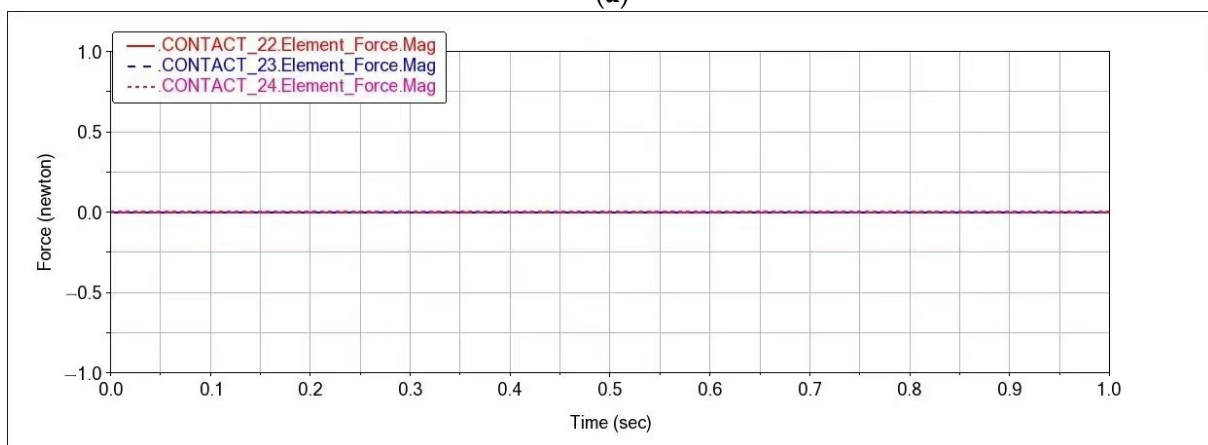

(**a**)

(**b**)

(**c**)

Figure 9. Simulation diagram of contact force between the divider and moderately lodged millet plant. (**a**) At 0.2 m of header height; (**b**) At 0.3 m of header height; (**c**) At 0.4 m of header height.
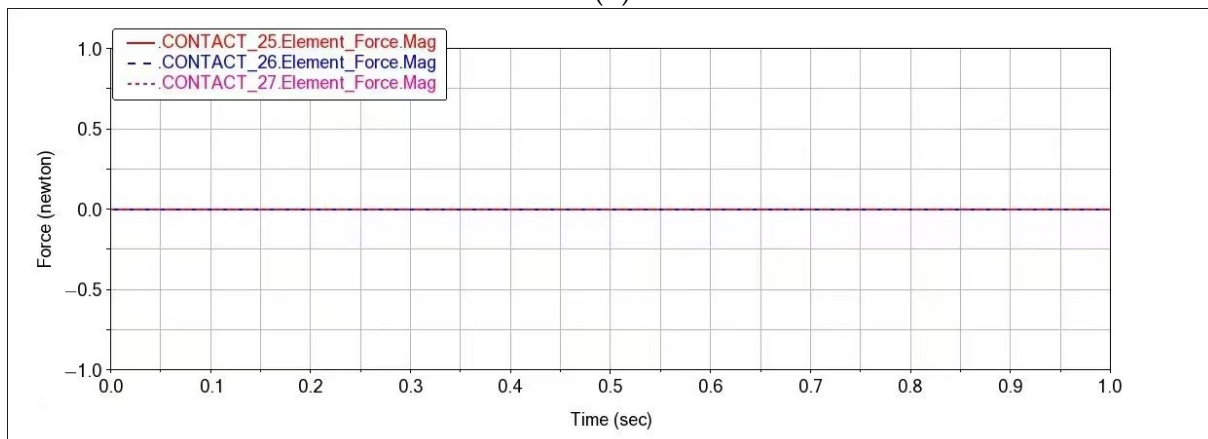
The contact stresses are shown in (a), (b), and (c) of Figures 11–13, and it can be observed that the stresses around the contact point and the lower part of the millet plant are higher during the contact between the divider and millet plant.

Figure 10. Simulation diagram of contact force between the divider and severely lodged millet plant. (**a**) At 0.2 m of header height; (**b**) At 0.3 m of header height; (**c**) At 0.4 m of header height.

At harvesting speed of 0.556 m·s⁻¹   At harvesting speed of 1.111 m·s⁻¹   At harvesting speed of 1.667 m·s⁻¹

(**a**)

At harvesting speed of 0.556 m·s⁻¹   At harvesting speed of 1.111 m·s⁻¹   At harvesting speed of 1.667 m·s⁻¹

(**b**)

At harvesting speed of 0.556 m·s⁻¹   At harvesting speed of 1.111 m·s⁻¹   At harvesting speed of 1.667 m·s⁻¹
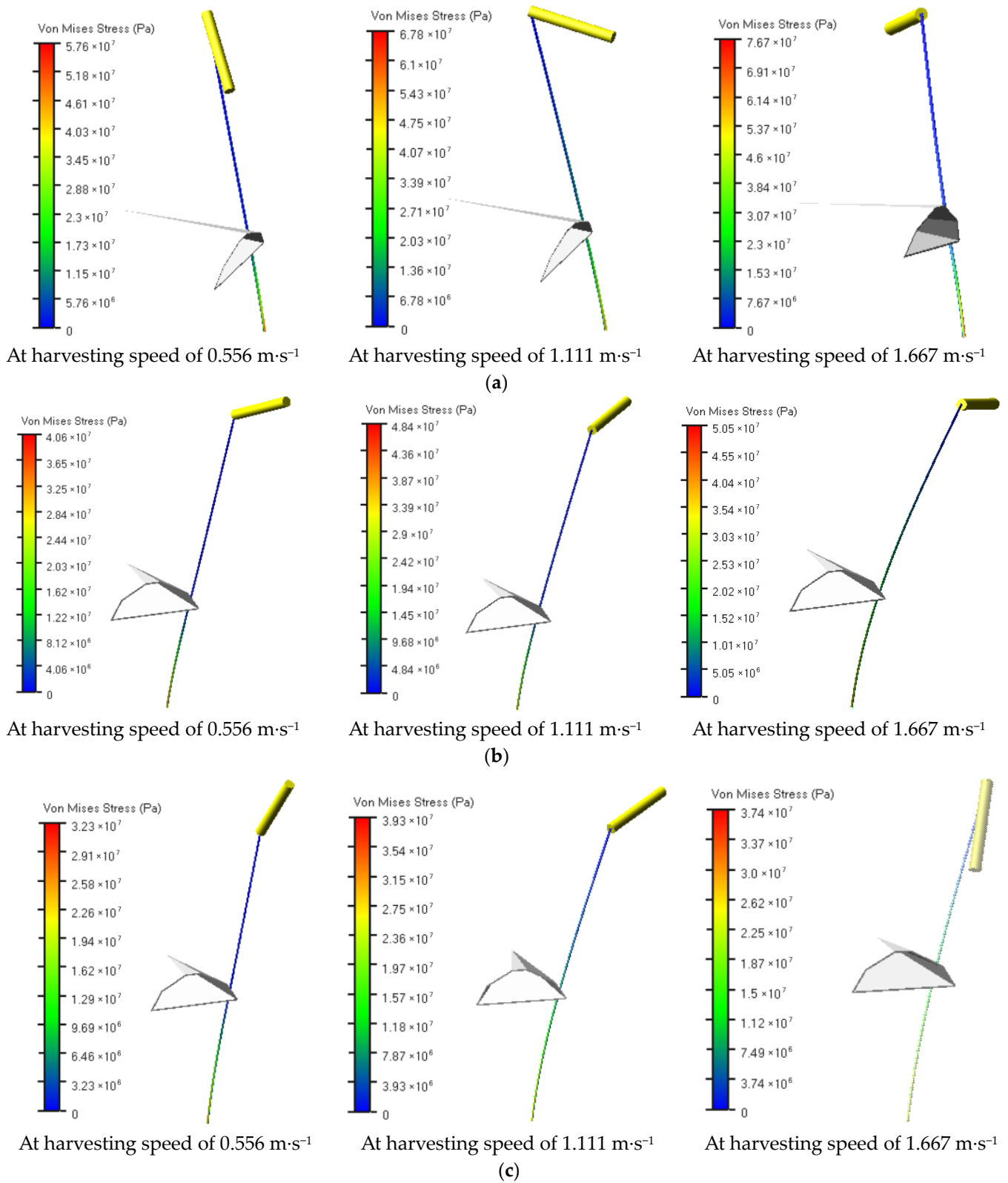
(**c**)

Figure 11. The stress of contact force between the divider and non-lodged millet plant. (**a**) At 0.2 m of header height; (**b**) At 0.3 m of header height; (**c**) At 0.4 m of header height.

At harvesting speed of 0.556 m·s⁻¹   At harvesting speed of 1.111 m·s⁻¹   At harvesting speed of 1.667 m·s⁻¹

(**a**)

At harvesting speed of 0.556 m·s⁻¹   At harvesting speed of 1.111 m·s⁻¹   At harvesting speed of 1.667 m·s⁻¹

(**b**)

At harvesting speed of 0.556 m·s⁻¹   At harvesting speed of 1.111 m·s⁻¹   At harvesting speed of 1.667 m·s⁻¹
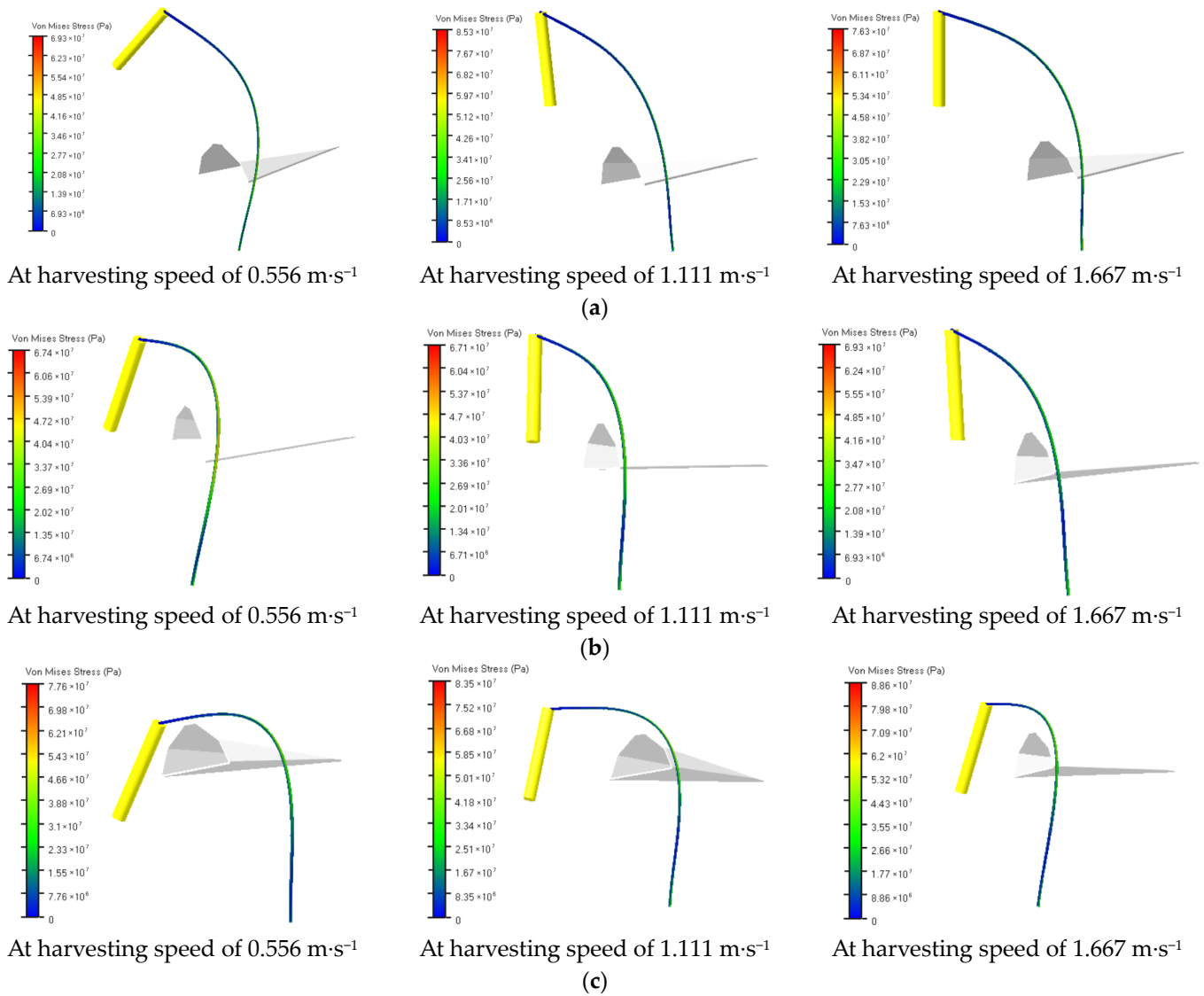
(**c**)

Figure 12. The stress of contact force between the divider and moderately lodged millet plant. (**a**) At 0.2 m of header height; (**b**) At 0.3 m of header height; (**c**) At 0.4 m of header height.

At harvesting speed of 0.556 m·s⁻¹   At harvesting speed of 1.111 m·s⁻¹   At harvesting speed of 1.667 m·s⁻¹
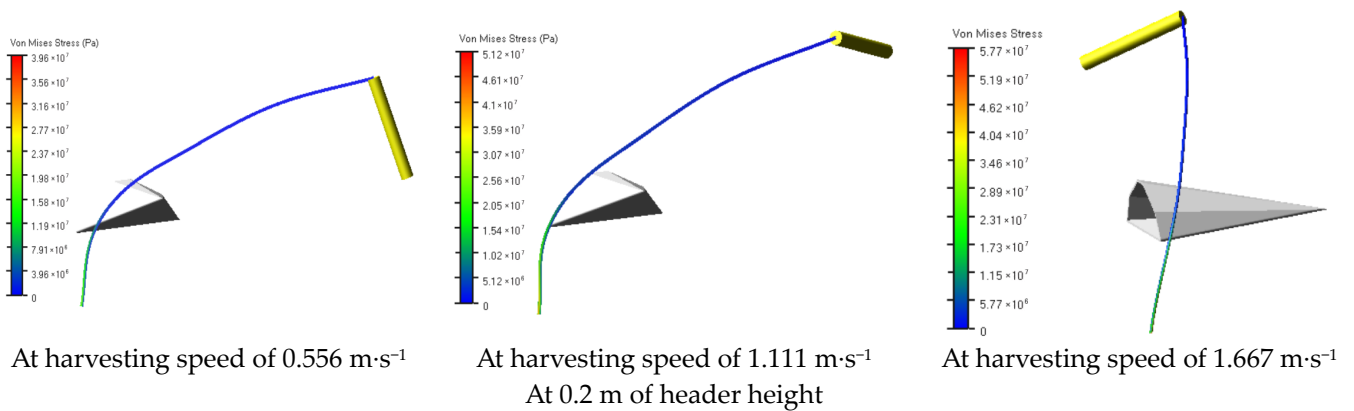
At 0.2 m of header height

Figure 13. The stress of contact force between the divider and severely lodged millet plant.

3.2. Analysis of Test Results

Using Design-Expert, the experimental indicators include the maximum contact force between the divider and non-lodged millet and the maximum Z-axis contact force between

the divider and millet with different lodging degrees. The results of the analysis of variance are presented in Table 6.

Table 6. Results of analysis of variance (ANOVA) of test indicators.

	Sources of Variance	Sum of Squares	Degrees of Freedom	Mean Square	F-Value	Pr > F
The maximum contact force between the divider and non-lodged millet plant	Model	85.67	4	21.42	64.18	0.0007
	A	74.85	2	37.43	112.15	0.0003
	B	10.82	2	5.41	16.21	0.0121
	Error	1.33	4	0.33		
	Sum	87.00	8			
The maximum Z-axis contact force for moderately lodged millet plant	Model	149.95	4	37.49	92.14	0.0003
	A	1.73	2	0.86	2.12	0.2352
	B	148.22	2	74.11	182.16	0.0001
	Error	1.63	4	0.41		
	Sum	151.58	8			
The maximum Z-axis contact force for severely lodged millet plant	Model	46.07	4	11.52	30.62	0.0029
	A	45.32	2	22.66	60.24	0.0010
	B	0.75	2	0.38	1.00	0.4444
	Error	1.50	4	0.38		
	Sum	47.57	8			

According to Table 6, it can be observed that, for the indicator of contact force between the divider and non-lodged millet plant, header height (Factor A) shows a highly significant effect, while harvesting speed (Factor B) shows a significant effect. Regarding the indicator of Z-directional contact force for moderately lodged millet plant, header height (Factor A) does not show a significant effect, while harvesting speed (Factor B) exhibits a highly significant effect. For the indicator of Z-directional contact force for heavily lodged millet plant, header height (Factor A) shows a highly significant effect, while harvesting speed (Factor B) does not show a significant effect.

In Table 6, the following are observed: The F values in the ANOVA of the maximum contact force between the divider and non-lodged millet plant were 112.15 and 16.21, respectively, indicating that the main factor influencing the maximum contact force between the divider and non-lodged millet plant was header height, followed by harvesting speed; the F values in the ANOVA of the maximum contact force between the divider and moderately lodged millet plant were 2.12 and 182.16, respectively, indicating that the main factor affecting the maximum contact force between the divider and moderately lodged millet plant was harvesting speed, and header height had almost no effect on the maximum contact force between the divider and moderately lodged millet plant; the F values in the ANOVA of the maximum contact force between the divider and severely lodged millet plant were 60.24 and 1.00, respectively, indicating that the main factor affecting the maximum contact force between the divider and severely lodged millet plant was header height, and harvesting speed had almost no effect on the maximum contact force between the divider and severely lodged millet plant.

Using the Optimization module in the Design-Expert software and following the principle of minimizing the contact force between the divider and non-lodged millet plant while maximizing the Z-directional contact force between the divider and millet plant at different lodging levels, the optimal parameters were determined. It was found that the best header performance was achieved when the header height was 0.2 m and the operating speed was 1.667 m·s^{-1}.

3.3. Field Experiment Results

The field experiments were conducted at Haifeng Farm in Fanshi, Shanxi, on 12–13 October 2023. The plots with flat terrain, less natural shattering, and no water accumulation

on the surface were selected to carry out the experiments to study the influence of various factors on the index. The testing methods referenced "Equipment for harvesting-Combine harvesters-Test procedure" [38] and "Agricultural machinery testing conditions-general rules for measuring methods" [39]. The experimental equipment mainly included a modified millet combine harvester, a single-chain header, a double-chain header, canvas, a tape measure, sealed bags, an electrically heated constant-temperature drying oven, etc. The variety tested was Zhangza 13 millet.

A complete experiment was conducted using the header height (factor A), harvesting speed (factor B), and header type (factor C) as influencing factors, and using the grain loss rate, ear loss rate, and total cutting loss rate as indicators, as shown in Table 7, repeated three times for each treatment.

Table 7. Header test parameters.

Treatment	A1	A2	A3	B1	B2	B3	C1	C2
Value	0.2 m	0.3 m	0.4 m	0.556 m·s^{-1}	1.111 m·s^{-1}	1.667 m·s^{-1}	Single-chain header	Double-chain header

The loss of cutting head directly reflects the performance of the header. The header loss includes grain loss and spike loss (i.e., shatter loss and dropped spike loss), as shown in Equation (11):

$$S_g = \frac{w_1 + w_2}{w} \times 100\% \tag{11}$$

where S_g is the header loss rate; w_1 is the grain loss of the header, g; w_2 is the loss of dropped spikes and unharvested spikes of the header, g; and w is the total mass of millet in the test area, g.

Collaborating with Weichai Lovol Intelligent Agricultural (Weifang, China) and Liaocheng Houde Electromechanical Co., Ltd. (Liaocheng, China), we improved the combine harvester suitable for millet harvesting. The experimental site of the grain combine harvester is shown in Figure 14, and the experimental results are shown in Table 8.

Figure 14. Millet harvesting experiment. Note: Shanxi Agricultural University Millet Industrialisation Technology Innovation Team.

Variance analysis was conducted on the experimental data, and the results are shown in Table 9.

Table 8. Loss rate of header.

Number	Header Height, m	Harvesting Speed (m·s^{-1})	Header Type	Grain Loss Rate S_l, %	Spike Loss Rate S_s, %	Total Header Loss Rate S_g, %
1	A1	B1	C1	0.71 ± 0.22 ab	6.55 ± 0.93 bc	7.26 ± 1.13 ab
2	A1	B1	C2	0.96 ± 0.23 a	2.35 ± 0.25 d	3.31 ± 0.48 c
3	A1	B2	C1	0.51 ± 0.11 bcd	5.80 ± 0.80 bc	6.31 ± 0.91 b
4	A1	B2	C2	0.68 ± 0.19 ab	2.73 ± 0.58 d	3.41 ± 0.73 c
5	A1	B3	C1	0.41 ± 0.11 bcde	5.45 ± 1.17 c	5.86 ± 1.22 b
6	A1	B3	C2	0.55 ± 0.21 bcd	2.57 ± 0.43 d	3.12 ± 0.62 c
7	A2	B1	C1	0.67 ± 0.19 abc	6.97 ± 0.51 abc	7.64 ± 0.69 ab
8	A2	B1	C2	0.72 ± 0.26 ab	3.06 ± 0.74 d	3.78 ± 0.74 c
9	A2	B2	C1	0.22 ± 0.06 de	6.70 ± 0.84 bc	6.92 ± 0.81 b
10	A2	B2	C2	0.51 ± 0.31 bcd	2.98 ± 0.35 d	3.49 ± 0.65 c
11	A2	B3	C1	0.38 ± 0.13 bcde	7.24 ± 0.33 ab	7.62 ± 0.43 ab
12	A2	B3	C2	0.26 ± 0.16 cde	3.06 ± 0.78 d	3.32 ± 0.64 c
13	A3	B1	C1	0.41 ± 0.10 bcde	8.42 ± 0.56 a	8.83 ± 0.65 a
14	A3	B1	C2	0.47 ± 0.22 bcde	3.70 ± 0.34 d	4.17 ± 0.12 c
15	A3	B2	C1	0.31 ± 0.11 bcde	7.16 ± 0.44 ab	7.47 ± 0.55 ab
16	A3	B2	C2	0.26 ± 0.13 cde	2.99 ± 0.19 d	3.25 ± 0.26 c
17	A3	B3	C1	0.07 ± 0.03 e	6.77 ± 1.43 bc	6.84 ± 1.45 b
18	A3	B3	C2	0.08 ± 0.05 e	3.42 ± 0.77 d	3.50 ± 0.81 c

Note: Different lowercase letters indicate significant differences between different treatments ($p < 0.05$).

Table 9. Results of analysis of variance of test indicators.

	Source of Variation	Sum of Squares	Degrees of Freedom	Mean Square	*F* Value	*Pr > F*
	Model	0.86	5	0.17	22.19	<0.0001
	A	0.41	2	0.21	26.51	<0.0001
Grain loss rate	B	0.41	2	0.21	26.68	<0.0001
S_l	C	0.036	1	0.036	4.59	0.0534
	Error	0.093	12	0.007		
	Sum	0.95	17			
	Model	69.96	5	13.99	74.89	<0.0001
	A	4.22	2	2.11	11.29	0.0017
Spike loss rate	B	0.76	2	0.38	2.04	0.1729
S_s	C	64.98	1	64.98	347.78	<0.0001
	Error	2.24	12	0.19		
	Sum	72.20	17			
	Model	66.24	5	13.25	65.02	<0.0001
	A	2.05	2	1.02	5.02	0.0260
Total header loss rate	B	2.21	2	1.11	5.43	0.0209
S_g	C	61.98	1	61.98	304.17	<0.0001
	Error	2.45	12	0.20		
	Sum	68.68	17			

As shown in Table 9, the influences of header height and harvesting speed on grain loss rate are extremely significant ($p < 0.01$), while the effect of header type on grain loss rate is not significant; the influences of header height and header type on spike loss rate are extremely significant ($p < 0.01$), while the effect of harvesting speed on spike loss rate is not significant; the influences of header height and harvesting speed on total header loss rate are significant ($p < 0.05$), while the effect of header type on total header loss rate is extremely significant ($p < 0.01$).

The impact on grain loss rate is ranked in descending order of harvesting speed, header height, and header type. The impact on grain loss rate is ranked in descending order of header type, header height, and harvesting speed. The impact on total header loss rate is ranked in descending order of header type, harvesting speed, and header height.

3.3.1. Effect of Header Height on Millet Harvester Header Loss Rate

At a harvesting speed of 1.11 m·s^{-1}, the grain loss rate, spike loss rate, and total header loss rate of millet harvested with different header heights and header types were analyzed, as shown in Figure 15.
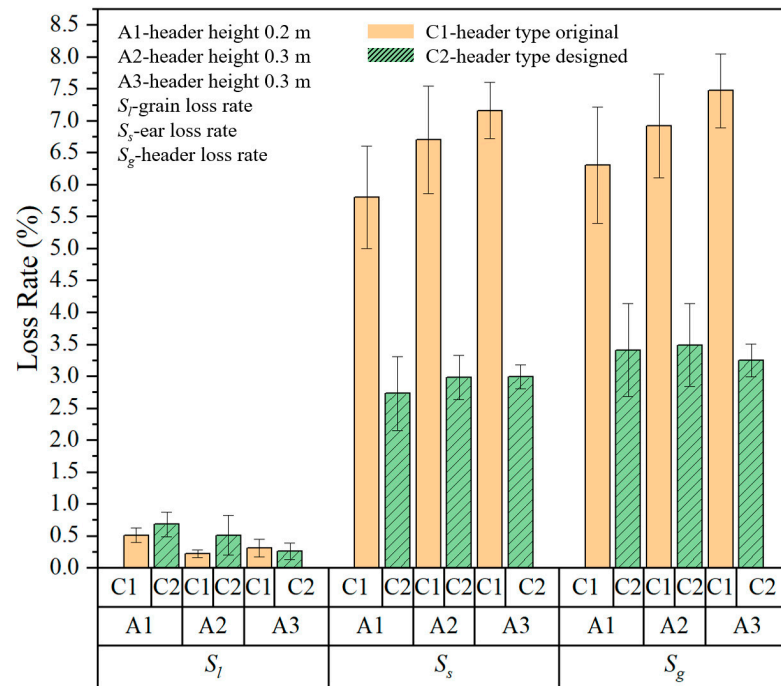

Figure 15. Relationship diagram between header heights and types of headers and header loss rate. Note: S_l is the grain loss rate, and Ss is the ear loss rate.

As shown in Figure 15, with the increase in header height, the grain loss rate of the single-chain header first decreases and then increases, reaching a minimum of 0.22% and a maximum of 0.51%; the spike loss rate shows an increasing trend, with a minimum of 5.80% and a maximum of 7.16%; the total header loss rate shows an increasing trend, with a minimum of 6.31% and a maximum of 7.47%. With the increase in header height, the grain loss rate of the double-chain header decreases, with a minimum of 0.26% and a maximum of 0.68%; the spike loss rate shows an increasing trend, with a minimum of 2.73% and a maximum of 2.99%; the total header loss rate first increases and then decreases, with a minimum of 3.25% and a maximum of 3.49%. When the harvesting speed is 1.111 m·s^{-1}, the total header loss rate of the double-chain header is much lower than that of the single-chain header under different header height conditions.

3.3.2. Effect of Harvesting Speed on Millet Harvester Header Loss Rate

At a header height of 0.3 m, the grain loss rate, spike loss rate, and total header loss rate of millet harvested with different harvesting speeds and different header types were analyzed, as shown in Figure 16.

As shown in Figure 16, with the increase in harvesting speed, the grain loss rate of the single-chain header first decreases and then increases, reaching a minimum of 0.22% and a maximum of 0.67%; the spike loss rate decreases first and then increases, with a minimum of 6.70% and a maximum of 7.24%; the total header loss rate decreases first and then increases, with a minimum of 6.92% and a maximum of 7.64%. With the increase in harvesting speed, the grain loss rate of the double-chain header decreases, with a minimum of 0.26% and a maximum of 0.72%; the spike loss rate decreases first and then increases, with a minimum of 2.98% and a maximum of 3.06%; the total header loss rate shows a decreasing trend, with a minimum of 3.32% and a maximum of 3.78%. When the header

height is 0.3 m, the total header loss rate of the double-chain header is much lower than that of the single-chain header under different harvesting speed conditions.
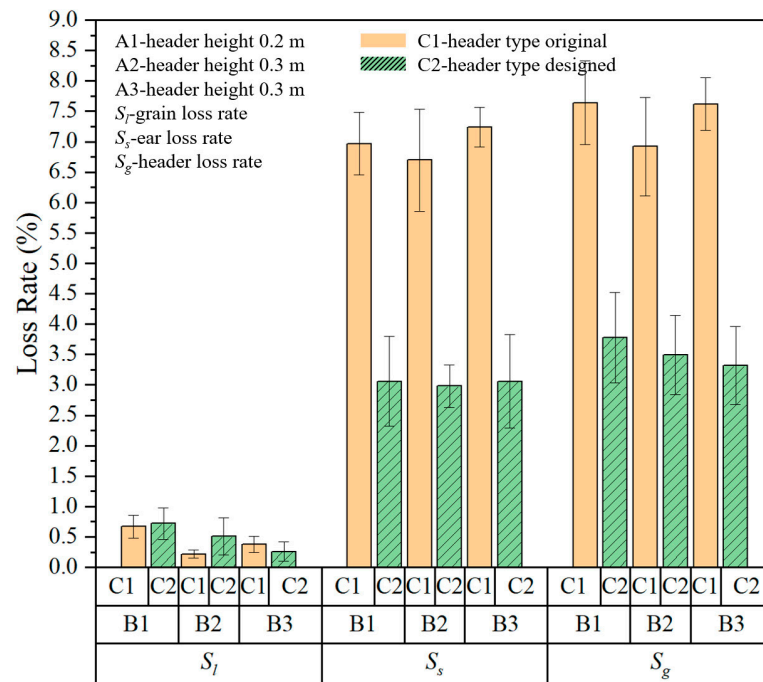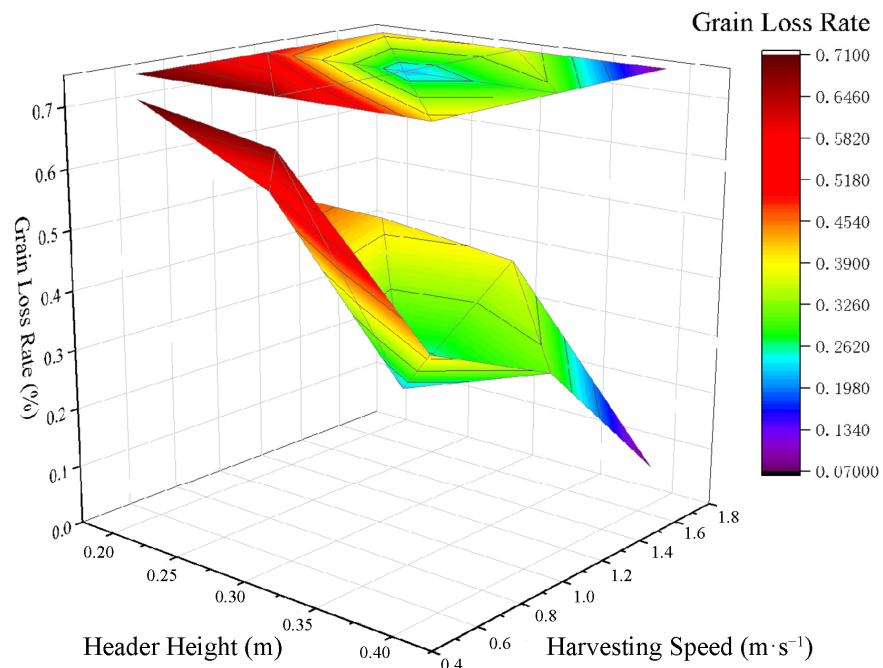

Figure 16. Relationship diagram between header speeds and types of headers and header loss rate.

An analysis was conducted on the interaction between different cutting heights and harvesting speeds on the grain loss rate, spike loss rate, and total cutting loss rate of millet, and the results are shown in Figures 17 and 18.

(**a**)

Figure 17. *Cont.*

(**b**)

(**c**)
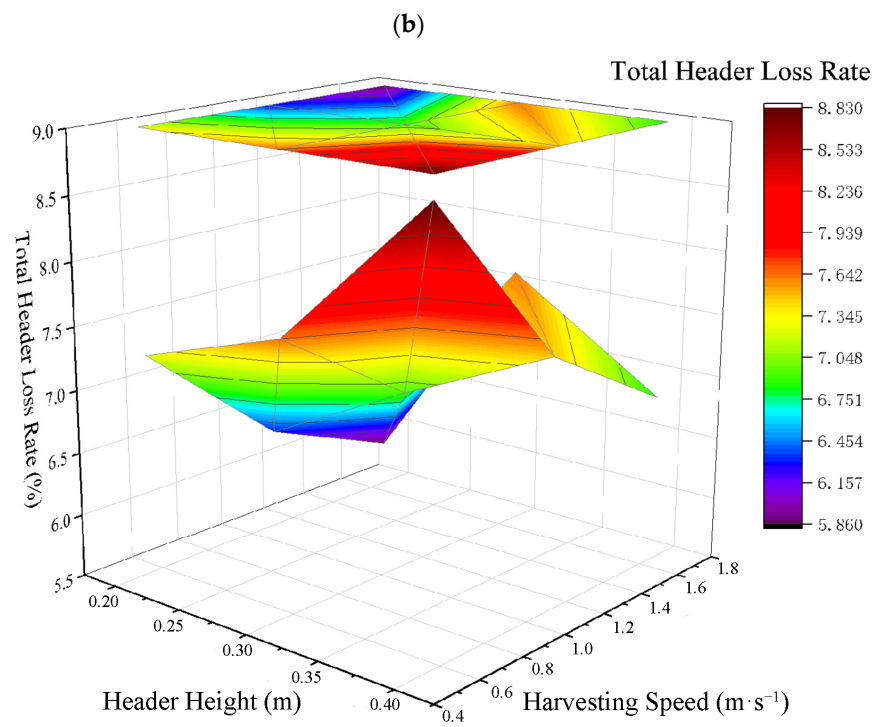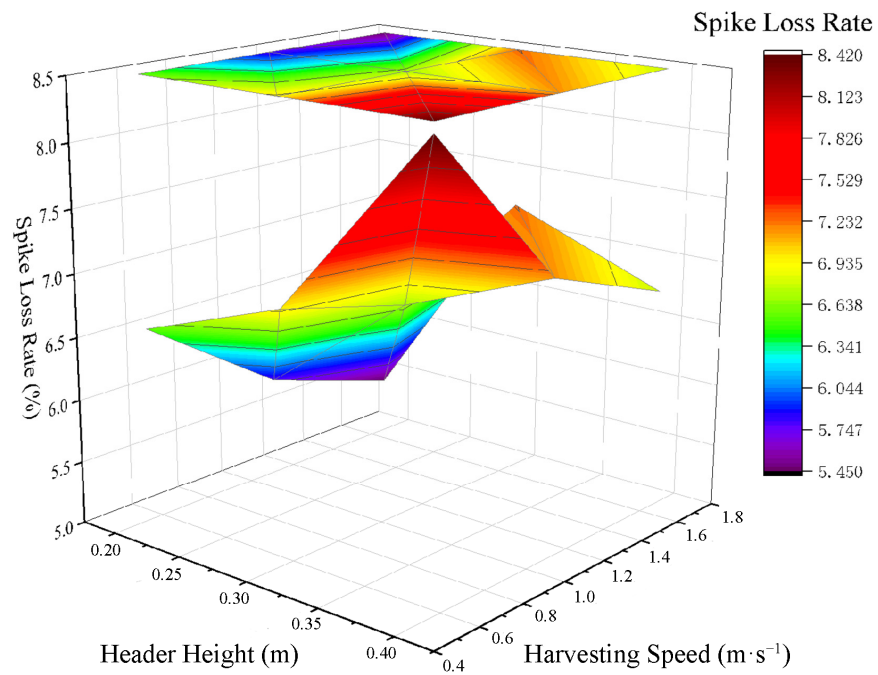
Figure 17. Graph depicting the correlation between factors and header loss rate for single-chain headers. (**a**) Graph depicting the relationship between header height, harvesting speed, and grain loss rate; (**b**) Graph illustrating the relationship between header height, harvesting speed, and spike loss rate; (**c**) Graph presenting the relationship between header height, harvesting speed, and total header loss rate.

According to Figure 17a, the grain loss rate of the single-chain header is highest when the header height is 0.2 m and the harvesting speed is 0.556 m·s^{-1}, reaching 0.71%. It is lowest when the header height is 0.4 m and the harvesting speed is 1.667 m·s^{-1}, at 0.07%. According to Figure 17b, the spike loss rate of the single-chain header is highest when the header height is 0.4 m and the harvesting speed is 0.556 m·s^{-1}, reaching 8.42%. It is lowest when the header height is 0.2 m and the harvesting speed is 1.667 m·s^{-1}, at 5.45%. According to Figure 17c, the total header loss rate of the single-chain header is highest when the header height is 0.4 m and the harvesting speed is 0.556 m·s^{-1}, reaching 8.83%. It is lowest when the header height is 0.2 m and the harvesting speed is 1.667 m·s^{-1}, at 5.86%.

According to Figure 18a, the grain loss rate of the double-chain header is highest when the header height is 0.2 m and the harvesting speed is 0.556 m·s^{-1}, reaching 0.96%. It is lowest when the header height is 0.4 m and the harvesting speed is 1.667 m·s^{-1}, at 0.08%. According to Figure 18b, the spike loss rate of the double-chain header is highest when the header height is 0.4 m and the harvesting speed is 0.556 m·s^{-1}, reaching 3.70%. It is lowest when the header height is 0.2 m and the harvesting speed is 0.556 m·s^{-1}, at 2.35%. According to Figure 18c, the total header loss rate of the double-chain header is highest when the header height is 0.4 m and the harvesting speed is 0.556 m·s^{-1}, reaching 4.17%. It is lowest when the header height is 0.2 m and the harvesting speed is 1.667 m·s^{-1}, at 3.12%.
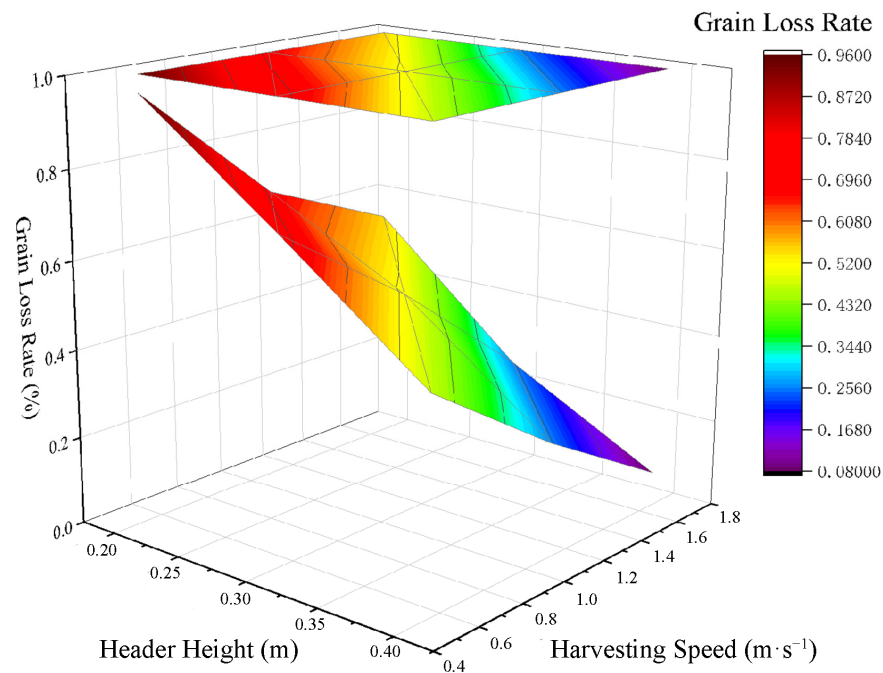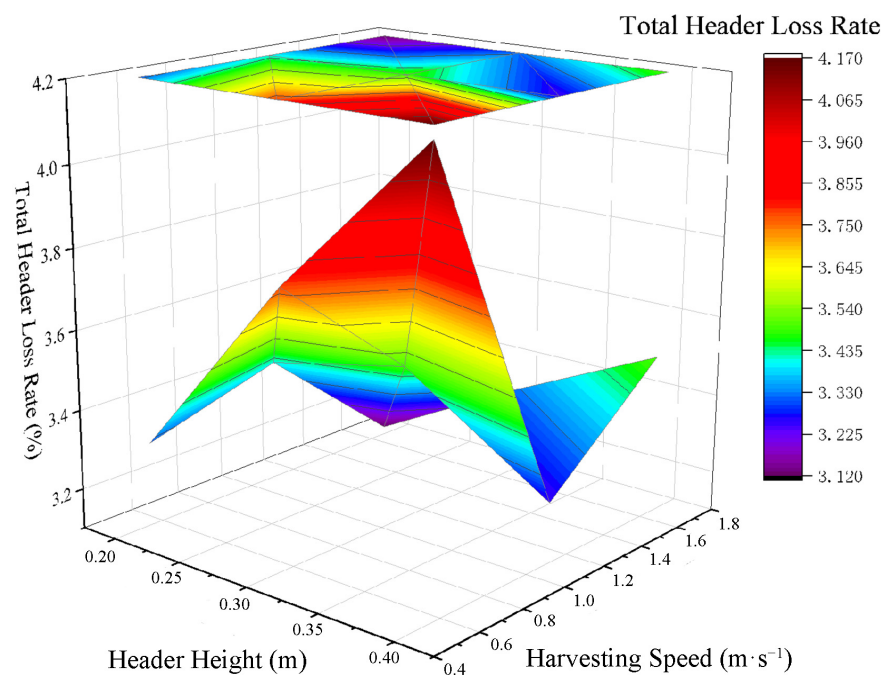

(**a**)

Figure 18. *Cont.*
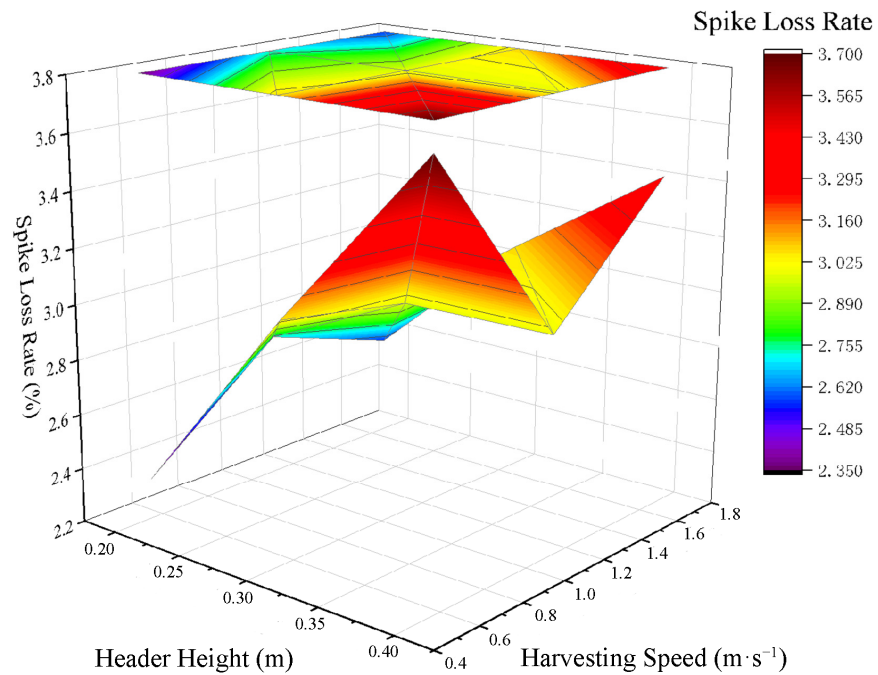
(**b**)

(**c**)

Figure 18. Graph depicting the correlation between factors and header loss rate for double-chain headers. (**a**) Graph depicting the relationship between header height, harvesting speed, and grain loss rate; (**b**) Graph illustrating the relationship between header height, harvesting speed, and spike loss rate; (**c**) Graph presenting the relationship between header height, harvesting speed, and total header loss rate.

3.3.3. Effect of Header Type on Millet Harvester Header Loss Rate

The analysis results of grain loss rate, spike loss rate, and total header loss rate of millet harvested with different header types at a header height of 0.3 m and harvesting speed of 1.111 m·s^{-1} are shown in Figure 19.
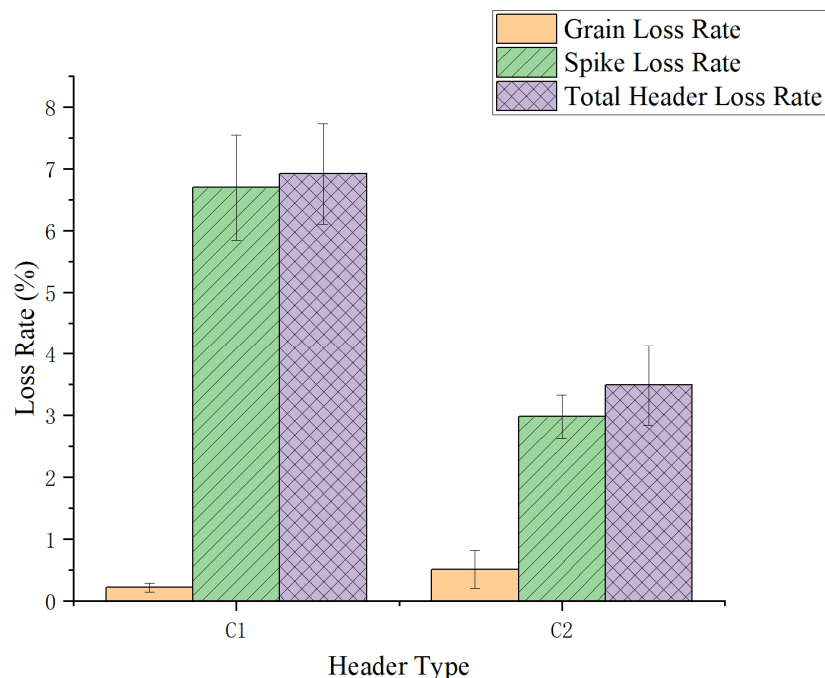
Figure 19. Relationship diagram between different header types and header loss rate.

As shown in Figure 19, the grain loss rate of the single-chain header is lower than that of the double-chain header, and the spike loss rate and the total header loss rate of the single-chain header are higher than those of the double-chain header.

When using a double-chain header with a header height of 0.2 m and a harvesting speed of 1.667 m·s^{-1}, the total header loss rate is the lowest, at 3.12%.

Studying the loss mechanism of the header during the combined harvest of millet is very important for the design and optimization of the header of the millet combine harvester. Tihanov et al. [40] established a linear correlation between grain loss percentage and the operational velocity of the combine harvester, suggesting that the predominant variability in grain loss is instigated by the operational speed of the combine harvester. Modak et al. [41] studied the effects of harvesting speed and cutting height on rice harvesting performance, which indicated that the harvesting speed and cutting height have significant effects on the cutting performance. Walter et al. [42] carried out harvest experiments on castor by using the reel-type and the straw baler-type headers, respectively, and the results showed that the straw baler-type header could significantly reduce the loss rate of the header. Our conclusion is consistent with the research results above. Based on the experiment of biological and mechanical properties of millet plants, the cutting head of the combine harvester suitable for millet harvesting was optimized and designed, and the parameters of key components of the header were determined. The field experiment showed that the loss rate of the header was effectively reduced.

The consistency between the simulation experiments and field experiments shows that our improved design is effective in reducing the loss rate of the millet harvester header.

4. Conclusions

To address the significant losses in millet combine harvester headers, a high-efficiency, low-loss, double-chain-type header was designed. This design was based on the study of the biological and mechanical properties of millet.

Using the principles of contact mechanics and tribology for agricultural materials and mechanical structures, the structural parameters of the header divider and the lifting cone were determined. The divider was 0.56 m long and 0.30 m wide, with a 40° divider angle. The maximum height of the stalk-lifting cone was 1.6 m, and its spiral angle was 40°.

The effects of cutting height, harvesting speed, and header type on the loss rate were analyzed. The results indicated that, at a header height of 0.2 m and a harvesting speed of 1.667 m/s, the double-chain header achieved the lowest loss rate of 3.12%. This significantly reduced the header loss in the millet combine harvester and provided a foundation for developing low-loss, high-efficiency millet combine harvesters.

References

1. Bandyopadhyay, T.; Singh, R.K.; Ramesh, P.; Maurya, J.; Prasad, M. The Promise of Millets in the Twenty-First Century: Emphasis on Breeding, Nutrition, Food Security and Sustainability. *J. Soil Sci. Plant Nutr.* **2022**, *23*, 628–637. [CrossRef]
2. Li, S.G.; Liu, F.; Liu, M.; Cheng, R.H.; Xia, E.J.; Diao, X.M. Current Status and Future Prospective of Foxtail Millet Production and Seed Industry in China. *Sci. Agric. Sin.* **2021**, *54*, 459–470.
3. Wang, F.; Liu, Y.; Li, Y.; Ji, K. Research and Experiment on Variable-Diameter Threshing Drum with Movable Radial Plates for Combine Harvester. *Agriculture* **2023**, *13*, 1487. [CrossRef]
4. Liang, Z.; Wada, M.E. Development of cleaning systems for combine harvesters: A review. *Biosyst. Eng.* **2023**, *236*, 79–102. [CrossRef]
5. Ding, B.; Liang, Z.; Qi, Y.; Ye, Z.; Zhou, J. Improving Cleaning Performance of Rice Combine Harvesters by DEM–CFD Coupling Technology. *Agriculture* **2022**, *12*, 1457. [CrossRef]
6. Luo, Y.; Wei, L.; Xu, L.; Zhang, Q.; Liu, J.; Cai, Q.; Zhang, W. Stereo-vision-based multi-crop harvesting edge detection for precise automatic steering of combine harvester. *Biosyst. Eng.* **2022**, *215*, 115–128. [CrossRef]
7. Cui, Y.S.; Qin, Y.F.; Wang, H.; Jiao, Z.Y.; Wang, L.G.; Han, K.C.; Ni, G.Q. Discussion on Millet Harvest Mechanization Technology. *Farm. Mach.* **2020**, *3*, 108–110.
8. Li, S.G.; Liu, F.; Zhao, W.Q.; Liu, M.; Xia, E.J.; Diao, X.M. The development history, integration models, and path selection for China's foxtail millet seed industry. *Res. Agric. Mod.* **2023**, *44*, 32–43.
9. Qiu, S.J.; Yuan, X.Y.; Zhang, Z.Q.; Zhao, Y.C.; Zhang, L. The effects of maturity period and harvesting methods on the harvesting performance of millet. *J. Shanxi Agric. Univ. Nat. Sci. Ed.* **2021**, *41*, 108–114.
10. Li, L.; Zhou, L.; Hao, J.H.; Chen, C. Research on the competitiveness of agricultural modernization in the context of the 20th National Congress of the Communist Party of China—Taking Nanjing, Jiangsu as an example. *J. Intell. Agric. Mech.* **2023**, *4*, 49–56, (In Chinese and English).
11. Pei, F.Q.; Yang, K.W.; Wang, M.; Tong, Y.F. Analysis of application status of intelligent manufacturing in agricultural machinery. *J. Intell. Agric. Mech.* **2022**, *3*, 7–19, (In Chinese and English).
12. Qian, Z.J.; Jin, C.Q.; Liu, Z.; Yang, T.X. Development status and trends of intelligent control technology in unmanned farms. *J. Intell. Agric. Mech.* **2023**, *4*, 1–13, (In Chinese and English).

13. Liang, S.N.; Jin, C.Q.; Zhang, F.F.; Kang, D.; Hu, M.J. Design and experiment of 4LZG-3.0 millet combine harvester. *Trans. Chin. Soc. Agric. Eng.* **2015**, *31*, 31–38.

14. Zheng, G.Q.; Li, Y.M.; Ji, K.Z.; Liang, Z.W.; Ma, X.; Cheng, J.H. Vibration analysis and structural optimization of header frame of millet combine harvester. *J. Agric. Mech. Res.* **2024**, *46*, 41–45+53.

15. Wang, R.X.; Chang, Y.P.; Li, B.; Lyu, W.Z.; Liu, J.L. Design and experiment on the key components of millet combine harvester header. *J. Agric. Mech. Res.* **2022**, *44*, 30–36.

16. Li, C. Design and Experimental Study on Low-Loss Header of Millet Combine Harvester. Master's Thesis, Henan University of Science and Technology, Luoyang, China, May 2019.

17. Zhang, X.M. The Design and Study on the Cutting Platform of Millet Combine Harvester. Master's Thesis, Shanxi Agricultural University, Jinzhong, China, June 2017.

18. Zhang, M.; Jin, M.; Wang, G.; Liang, S.N.; Wu, C.Y. Design and Test of Double Crank Planar Five-bar Reel in Rape Windrower. *Trans. Chin. Soc. Agric. Mach.* **2022**, *53*, 115–122.

19. Chen, H.T.; Dun, G.Q. Optimization of parameters for soybean lifter based on dynamic simulation of virtual prototype. *Trans. Chin. Soc. Agric. Eng.* **2012**, *28*, 23–29.

20. Gu, L.L.; Cao, W.B.; Sun, W.L.; Liu, J.D.; Tian, D.Y.; Ma, P. Motion Simulation and Design of Safflower Harvester Crop Lifter Adjustment Mechanism. *J. Agric. Mech. Res.* **2018**, *40*, 17–21.

21. Guo, J.D.; Wu, D.L.; Chen, L.Q. Simulation of Maize Culm with Harvester Header Based on ADAMS. *J. Agric. Mech. Res.* **2016**, *38*, 80–85+100.

22. Hu, Z.C.; Wang, H.O.; Peng, B.L.; Chen, Y.Q.; Wu, F.; Xie, H.X. Performance analysis and experiment on operation process of plant lifting device in 4HLB-2 type peanut combine harvester. *Trans. Chin. Soc. Agric. Eng.* **2012**, *28*, 26–31.

23. Liu, W.; Huang, X.M.; Ma, L.N.; Zong, W.Y.; Zhu, Y.F. Design and Experiment of Special Header of Oil Sunflower Combine Harvester. *Trans. Chin. Soc. Agric. Mach.* **2020**, *51*, 83–88+135.

24. Shu, C.X.; Cao, S.C.; Liao, Y.T.; Liao, Q.X.; Wan, X.Y.; Li, Y.T. Parameter Optimization and Experiment of Forward Laying Device for Rape Windrower Based on ADAMS. *Trans. Chin. Soc. Agric. Mach.* **2022**, *53*, 11–19+38.

25. Liu, W.; Zeng, S.; Chen, X. Design and Experiment of Adaptive Profiling Header Based on Multi-Body Dynamics–Discrete Element Method Coupling. *Agriculture* **2024**, *14*, 105. [CrossRef]

26. Pang, J.; Li, Y.; Ji, J.; Xu, L. Vibration excitation identification and control of the cutter of a combine harvester using triaxial accelerometers and partial coherence sorting. *Biosyst. Eng.* **2019**, *185*, 25–34. [CrossRef]

27. Ma, Z.; Zhu, Y.; Chen, S.; Traore, S.N.; Li, Y.; Xu, L.; Shi, M.; Zhang, Q. Field Investigation of the Static Friction Characteristics of High-Yielding Rice during Harvest. *Agriculture* **2022**, *12*, 327. [CrossRef]

28. Wang, Z.X.; Wang, L.H.; Xu, N.H.; Li, Y.; Shi, J.C. Research on the control strategy of sideslip and hysteresis of intelligent harvesting robot. *J. Intell. Agric. Mech.* **2022**, *3*, 37–44, (In Chinese and English).

29. Wang, Y.K. Design and Virtual Experiment Research on Key Components of Corn Harvester Plate Header. Master's Thesis, Shandong Agricultural University, Taian, China, May 2021.

30. Li, L.; Gan, Z.Y.; Li, C.B.; Li, L.L.; Liu, J.W.; Wang, H.J. Design parameter optimization method of screw conveyor for high efficiency and energy saving. *Comput. Integr. Manuf. Syst.* **2023**, *29*, 2585–2594.

31. Sosa-Méndez, D.; Lugo-González, E.; Arias-Montiel, M.; García-García, R.A. ADAMS-MATLAB co-simulation for kinematics, dynamics, and control of the Stewart–Gough platform. *Int. J. Adv. Robot. Syst.* **2017**, *4*, 1729881417719824. [CrossRef]

32. Li, H.B.; Xue, J.X.; Wang, B.X.; Zhang, Y.Q.; Wu, X.H.; Li, X.B.; Cui, Q.L.; Yang, Z.M. Tensile properties of foxtail millet leaf sheath, leaf and leaf collar. *Trans. Chin. Soc. Agric. Eng.* **2020**, *36*, 11–17.

33. Zhang, L. The Influence of Header Parameters on the Quality of Foxtail Millet Harvest in a Grain Combine Harvester. Master's Thesis, Shanxi Agricultural University, Taian, China, June 2021.

34. Wang, G.X.; Ma, D.L.; Liu, Y.; Liu, C.S. Research progress of contact force models in the collision mechanics of multibody system. *Chin. J. Theor. Appl. Mech.* **2022**, *54*, 3239–3266.

35. Du, Y.; Mao, E.; Song, Z.; Zhu, Z.; Gao, J. Simulation on Corn Plants in Harvesting Process Based on ADAMS. *Trans. Chin. Soc. Agric. Mach.* **2012**, *Z1*, 106–111.

36. Vishwas, J.; Anuja-Ria, J. Two-factor, Three-level Factorial Experiments for Optimizing Size of Thiol Stabilized Gold Nanoparticles (AuNPs). *Microsc. Microanal.* **2023**, *29*, 2068–2069. [CrossRef]

37. Ge, Y.Y. Analysis of Variance. In *Experimental Design Methods and Application of Design-Expert Software*; Wang, J.F., Ed.; Harbin Institute of Technology Press: Harbin, China, 2014; pp. 36–60. ISBN 978-7-5603-4992-3.

38. *GB/T 8097-2008*; Test Method for Harvesting Machinery Combine Harvester. General Administration of Quality Supervision, Inspection and Quarantine of the People's Republic of China, China National Standardization Administration: Beijing, China, 2008.

39. *GB/T 5262-2008*; Agricultural Machinery Testing Conditions-General Rules for Measuring Methods. General Administration of Quality Supervision, Inspection and Quarantine of the People's Republic of China, China National Standardization Administration: Beijing, China, 2008.

40. Tihanov, G.; Dallev, M.; Hristova, G.; Mitkov, I. Loss of grain at harvesting wheat with a combine harvester. *Series A Agron.* **2021**, *64*, 577–582.

41. Modak, S.; Raheman, H. Effects of Various Machine Parameters on Cutting Performance for High-speed Cutting of Paddy Crop. *J. Biosyst. Eng.* **2022**, *47*, 181–196. [CrossRef]

42. Stefanoni, W.; Latterini, F.; Malkogiannidis, V.; Salpiggidis, V.; Alexopoulou, E.; Pari, L. Mechanical Harvesting of Castor Bean (*Ricinus communis* L.) with a Combine Harvester Equipped with Two Different Headers: A Comparison of Working Performance. *Energies* **2022**, *15*, 2999. [CrossRef]